



The transcriptional coactivator TAZ regulates reciprocal differentiation of T_H17 cells and T_{reg} cells

Jing Geng^{1,6}, Shujuan Yu^{1,6}, Hao Zhao^{1,6}, Xiufeng Sun^{1,6}, Xun Li², Ping Wang¹, Xiaolin Xiong¹, Lixin Hong¹, Changchuan Xie¹, Jiahui Gao¹, Yiran Shi¹, Jiaqi Peng¹, Randy L Johnson³, Nengming Xiao¹, Linrong Lu^{4,5} , Jiahui Han¹, Dawang Zhou¹  & Lanfen Chen¹

An imbalance in the lineages of immunosuppressive regulatory T cells (T_{reg} cells) and the inflammatory T_H17 subset of helper T cells leads to the development of autoimmune and/or inflammatory disease. Here we found that TAZ, a coactivator of TEAD transcription factors of Hippo signaling, was expressed under T_H17 cell-inducing conditions and was required for T_H17 differentiation and T_H17 cell-mediated inflammatory diseases. TAZ was a critical co-activator of the T_H17-defining transcription factor ROR γ t. In addition, TAZ attenuated T_{reg} cell development by decreasing acetylation of the T_{reg} cell master regulator Foxp3 mediated by the histone acetyltransferase Tip60, which targeted Foxp3 for proteasomal degradation. In contrast, under T_{reg} cell-skewing conditions, TEAD1 expression and sequestration of TAZ from the transcription factors ROR γ t and Foxp3 promoted T_{reg} cell differentiation. Furthermore, deficiency in TAZ or overexpression of TEAD1 induced T_{reg} cell differentiation, whereas expression of a transgene encoding TAZ or activation of TAZ directed T_H17 cell differentiation. Our results demonstrate a pivotal role for TAZ in regulating the differentiation of T_{reg} cells and T_H17 cells.

Naive CD4⁺ T cells can differentiate into distinct helper T cell subsets, including T_H1, T_H2 and T_H17 cells, as well as Foxp3⁺ regulatory T cells (T_{reg} cells)^{1,2}. The T_H17 cell and T_{reg} cell subsets have emerged as major participants in autoimmunity. T_H17 cells represent a pro-inflammatory subset that can contribute to autoimmunity and tissue damage. In contrast, T_{reg} cells are immunosuppressive and prevent autoimmunity. The developmental pathways for T_H17 cells and T_{reg} cells are reciprocally interconnected, and there is plasticity between the T_H17 cell lineage and T_{reg} cell lineage^{3–8}. Thus, understanding the mechanism that control the balance of immunosuppressive T_{reg} cells and inflammatory T_H17 cells would help in the development of therapeutics for intervention during system failures in autoimmunity and chronic inflammation. The cytokine TGF- β drives the conversion of naive T cells into T_{reg} cells, while TGF- β , together with pro-inflammatory cytokines, including IL-6 and IL-21, differentiates T cells into T_H17 cells². Mechanistically, TGF- β alone can activate its downstream transcription factors Smad2 and Smad3 to induce expression of the transcription factor Foxp3, which is essential for the generation of T_{reg} cells. In contrast, IL-6 activates the cascade of the kinase JAK and transcription factors STAT3 and STAT5 to induce expression of the T_H17 cell-defining transcriptional factor ROR γ t critical for IL-17 expression. Notably, TGF- β alone induces the expression of both Foxp3 and ROR γ t but not that of IL-17 (ref. 4), which indicates that some as-yet-unknown effectors downstream of TGF- β –IL-6 signaling

function to coordinate the transcriptional activities of Foxp3 and ROR γ t. The transcriptional coactivator TAZ ('transcriptional coactivator with postsynaptic density 65-discs large-zonula occludens 1-binding (PDZ) motif') has pivotal roles in the differentiation of mesenchymal stem cells, organ-size control and cancer development^{9–12}. In response to TGF- β , TAZ promotes the accumulation of Smad proteins in the nucleus and their activation^{13,14}. TAZ and its paralog, YAP ('Yes (proto-oncogene product)-associated protein'), are regulated mainly by the Hippo tumor-suppressor pathway^{15–19}. The Ste20 (mitogen-activated protein kinase kinase kinase)-like kinases MST1 and MST2 (collectively called 'MST1/2' here) are key components of the mammalian Hippo signaling pathway, along with the scaffolding protein WW45, kinases of the NDR family (NDR1, NDR2, LATS1 and LATS2), and the adaptor MOB1. MST1/2 phosphorylates and activates LATS1–LATS2–MOB1, which then phosphorylates their downstream effectors YAP and TAZ. Phosphorylated TAZ (or YAP) is either degraded or is sequestered in the cytoplasm by the adaptor 14-3-3 (ref. 20). When the Hippo pathway is switched off, TAZ (or YAP) translocates to the nucleus and forms a functional transcriptional complex with transcription factors of the TEAD ('TEA-ATTS DNA-binding domain') family (TEAD1–TEAD4) to turn on pro-proliferative genes. Although the role of the Hippo signaling cascade in cell-growth control has been studied extensively, it is less well appreciated that MST1 deficiency in humans and mice results

¹State Key Laboratory of Cellular Stress Biology, Innovation Center for Cell Signaling Network, School of Life Sciences, Xiamen University, Xiamen, Fujian, China. ²Department of Laboratory Medicine, the First Affiliated Hospital, Medical College of Xiamen University, Xiamen, China. ³Department of Cancer Biology, Maryland Anderson Cancer Center, University of Texas, Houston, Texas, USA. ⁴Institute of Immunology, Innovation Center for Cell Signaling Network, Zhejiang University School of Medicine, Hangzhou, China. ⁵Zhejiang University–University of Edinburgh Institute, Zhejiang University School of Medicine, Hangzhou, China. ⁶These authors contributed equally to this work. Correspondence should be addressed to D.Z. (dwzhou@xmu.edu.cn) or L.C. (chenlanfen@xmu.edu.cn).

Received 21 December 2016; accepted 20 April 2017; published online 15 May 2017; doi:10.1038/ni.3748

in a complex combined immunodeficiency syndrome with autoimmune manifestations^{21–23}. Studies have indicated that this pathway regulates the migration and activation of T cells and is also essential in innate immunity and cancer immunity^{24–42}. However, the role of Hippo signaling in T cell differentiation is as yet largely unexplored. Here we found that TAZ, but not YAP, was induced exclusively in the T_H17 cell lineage and that TAZ was required for T_H17 differentiation and T_H17 cell-mediated inflammatory diseases. Our results identified TAZ as a critical co-activator of the T_H17 cell-defining transcriptional factor ROR γ t. In addition, TAZ attenuated T_{reg} cell development by decreasing acetylation of the T_{reg} cell master regulator Foxp3 mediated by the histone acetyltransferase Tip60, and targeted Foxp3 for proteasomal degradation. In contrast, T_{reg} cell-skewing triggered high expression of TEAD1, which sequestered TAZ from ROR γ t, Tip60 and Foxp3 to promote T_{reg} cell differentiation. Thus, TEAD functions as an antagonist of TAZ directed against T_H17 differentiation. Notably, TAZ deficiency induced T_{reg} cell differentiation, whereas expression of a transgene encoding TAZ or activation of TAZ directed T_H17 cell differentiation. Our results demonstrate that TAZ functions as a cell-fate switch between the immunosuppressive T_{reg} cell lineage and the inflammatory T_H17 cell lineage.

RESULTS

Substantial enrichment for TAZ in the T_H17 cell subset

To explore the role of MST1/2 in the activation and differentiation of T cells, we generated mice with conditional deletion of MST1/2 in activated T cells by crossing mice homozygous for *loxP*-flanked alleles encoding MST1 and MST2 (*Mst1^{fl/fl}Mst2^{fl/fl}*) with mice with transgenic expression of Cre recombinase from the gene encoding OX40 (*Tnfrsf4*; called ‘Ox40’ here), a marker of activated T cells (*Ox40-Cre*). *Mst1^{fl/fl}Mst2^{fl/fl}Ox40-Cre* mice exhibited normal T cell development in the thymus (Supplementary Fig. 1a) and normal numbers of T cells in peripheral lymphoid tissues, but slightly more effector-memory T cells in the spleen than those of their *Mst1^{fl/fl}Mst2^{fl/fl}* littermates (Supplementary Fig. 1b–d). Next, we immunized *Mst1^{fl/fl}Mst2^{fl/fl}Ox40-Cre* mice and their *Mst1^{fl/fl}Mst2^{fl/fl}* littermates with keyhole limpet hemocyanin (KLH) in complete Freund’s adjuvant. After 1 week, a comprehensive analysis of the lymphocytes from draining lymph nodes by mass cytometry was performed. Notably, knockout of MST1/2 resulted in a substantial increase in the frequency of T_H17 cells and a modest decrease in the frequency of T_{reg} cells (Fig. 1a). Also notably, real-time PCR analysis of genes encoding the components of the Hippo pathway showed that *Taz* mRNA, but not *Yap1* mRNA, was robustly induced in both T_{reg} cells and T_H17 cells but underwent the greatest induction in T_H17 cells (Fig. 1b). *Tead1* mRNA was much more abundant in T_{reg} cells than in T_H0 cells but was undetectable in other subsets analyzed (Fig. 1b). The increased expression of TAZ in T_H17 cells and T_{reg} cells was confirmed by immunoblot analysis (Fig. 1c). Furthermore, TAZ-deficient mice (generated by crossing of *Taz^{fl/fl}* mice with mice expressing Cre from the gene encoding the T cell-specific tyrosine kinase Lck (*Lck-Cre*): *Taz^{fl/fl}Lck-Cre* mice) immunized with KLH exhibited a larger T_H17 population and fewer T_{reg} cells than that of their *Taz^{fl/fl}* littermates, but their YAP-deficient counterparts did not (Fig. 1d,e and data not shown). Moreover, *Mst1^{-/-}* mice were prone to autoimmune diseases, such as Sjögren’s syndrome, with associated infiltration of the lacrimal gland by lymphocytic cells (Supplementary Fig. 1e). Consistent with that, real-time PCR analysis revealed substantially higher expression of *Taz* and T_H17 signature genes in the lacrimal glands of *Mst1^{-/-}* mice than in those of *Mst1^{+/+}* mice (Supplementary Fig. 1f). Notably, *RORC* (which encodes ROR γ t) and TAZ had higher coexpression in

memory CD4⁺ T cells isolated from the peripheral blood of patients with rheumatoid arthritis or Sjögren’s syndrome disease than in that of healthy people (Fig. 1f,g and Supplementary Table 1). In addition, higher TAZ expression was also observed in human T_H17 and T_{reg} cells, but not in T_H1 cells or T_H2 cells, relative to its expression in T_H0 cells (Fig. 1h). Therefore, we speculated that TAZ might serve a critical role downstream of the kinases MST1 and MST2 in autoimmunity via regulation of the T_{reg} cell and T_H17 cell lineages.

TAZ is dispensable in T cell activation and proliferation

To further determine the function of TAZ in T cells, we analyzed mice with T cell-specific knockout of TAZ (*Taz^{fl/fl}Lck-Cre* mice; called ‘TAZ-cKO mice’ here). There were no gross differences between *Taz^{fl/fl}* mice (called ‘wild-type mice’ here) and TAZ-cKO mice in their T cell subsets in the thymus, lymph nodes and spleen (Supplementary Fig. 2a–c). Moreover, peripheral CD4⁺ T cells in wild-type and TAZ-cKO mice showed similar expression of the activation markers CD62L (L-selectin) and CD44 (Supplementary Fig. 2b,d). Expression of the activation markers CD69, CD25, CD62L and CD44 on CD4⁺ T cells, as well as production of the cytokines IL-2 and IFN- γ , were unaffected by the deletion of *Taz* when assessed after stimulation via the T cell antigen receptor (TCR) with antibody to the invariant signaling protein CD3 (anti-CD3) or with anti-CD3 plus antibody to the costimulatory receptor CD28 (anti-CD28) (Supplementary Fig. 2e,f). TAZ acts as a transcriptional co-activator of TEAD transcription factors to promote cell proliferation. However, wild-type and TAZ-cKO CD4⁺ T cells, T_H17 cells and T_{reg} cells showed similar proliferation rates after stimulation with anti-CD3 plus anti-CD28 (Supplementary Fig. 2g,h). Together these results indicated that the TCR-induced signaling cascade was intact in TAZ-deficient T cells and that TAZ was dispensable for the activation and proliferation of naive T cells.

TAZ drives T_H17 differentiation but blocks T_{reg} differentiation

To assess whether TAZ is involved in regulating commitment to the helper T cell lineage, we differentiated wild-type or TAZ-cKO naive CD4⁺ T cells under T_H17-, T_{reg} cell- or T_H1-polarizing conditions. Notably, TAZ deficiency resulted in a significantly lower frequency of IL-17⁺ cells without affecting ROR γ t expression and a higher frequency of Foxp3⁺ cells, after T_H17 skewing (Fig. 2a and Supplementary Fig. 2i,j). Knockout of TAZ also led to decreased expression of the cytokines IL-17A, IL-17F and GM-CSF and the cytokine receptor IL-23R (Fig. 2a and Supplementary Fig. 2i,j). In addition, TAZ deficiency resulted in much greater frequency of Foxp3⁺ cells than that of wild-type Foxp3⁺ cells, after T_{reg} cell skewing (Fig. 2b), and a frequency of IFN- γ ⁺ cells and IFN- γ production comparable to that of wild-type and TAZ-cKO naive CD4⁺ T cells, after T_H1 skewing (Fig. 2c). Consistent with that, considerably fewer T_H17 cells and many more T_{reg} cells were present in the intestinal lamina propria (LP) of TAZ-cKO mice than in that of wild-type mice (Fig. 2d), which suggested that TAZ deficiency impaired the generation of T_H17 cells and facilitated the differentiation of T_{reg} cells *in vivo*. Furthermore, overexpression of TAZ resulted in enhanced T_H17 differentiation but attenuated T_{reg} cell differentiation, and reintroduction of TAZ into TAZ-cKO T cells ‘rescued’ the TAZ-deficient phenotypes (Fig. 2e). Thus TAZ had a critical role in balancing Foxp3 activity and ROR γ t activity during the development of T_H17 cells and T_{reg} cells.

TAZ-enhanced development of T_H17 cell-driven autoimmunity

Next we sought to explore the role of TAZ in the development of T_H17 cell-mediated inflammatory disease. We first immunized

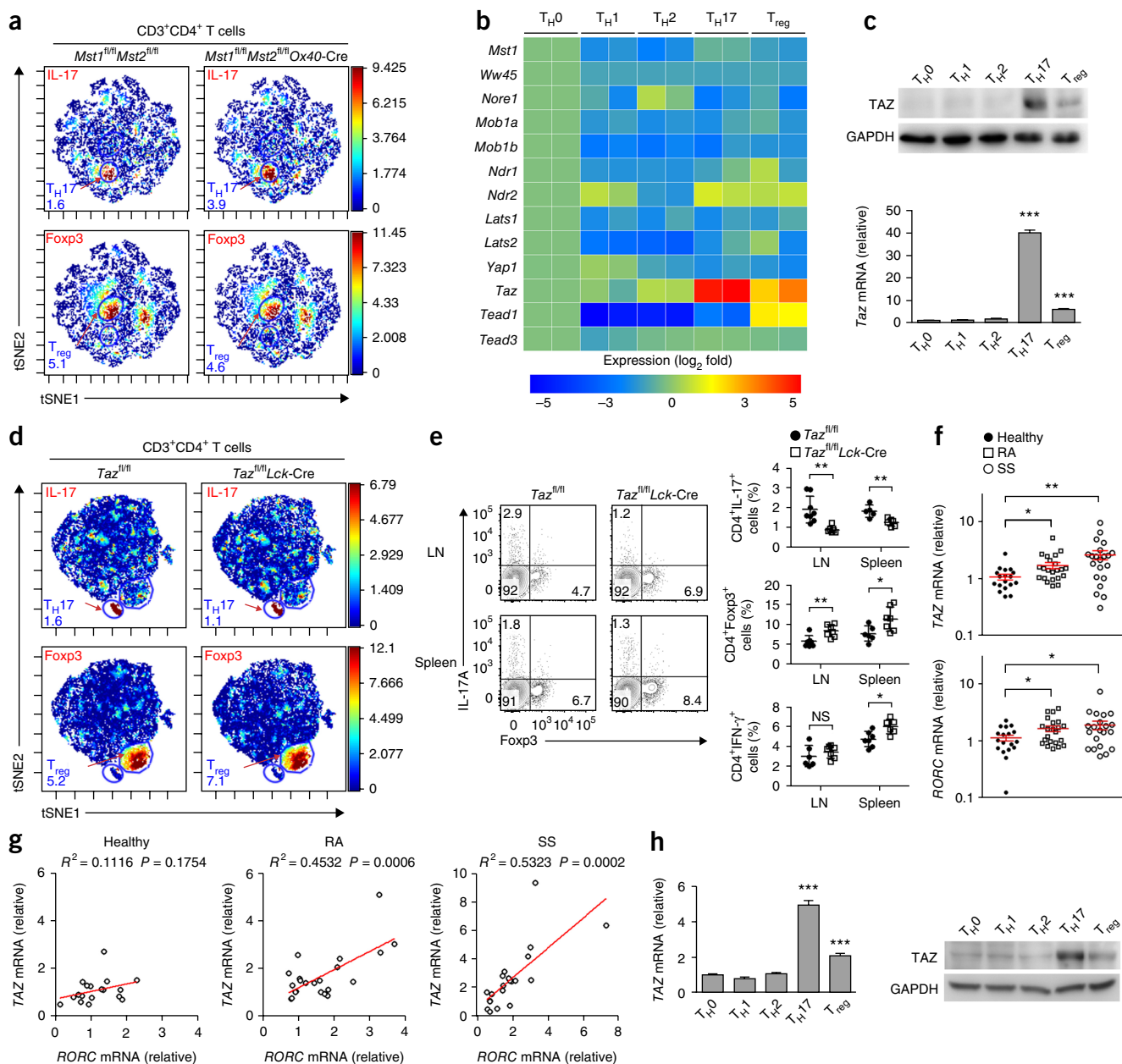


Figure 1 The T_{H17} subset shows enrichment for TAZ, and TAZ is associated with T_{H17} cell-mediated autoimmune diseases. **(a)** Visualization and mapping (with the viSNE algorithm) of CD3⁺CD4⁺ T cells from the draining lymph nodes of KLH-treated *Mst1^{fl/fl}Mst2^{fl/fl}* and *Mst1^{fl/fl}Mst2^{fl/fl}Ox40-Cre* mice (above plots) analyzed by mass cytometry; colors indicate intensity of expression (key, right margin) of the markers IL-17 and Foxp3 (top left corners). Numbers in plots (bottom left corner) indicate percent T_{H17} cells (top row) or T_{reg} cells (bottom row); red arrows indicate those subsets. **(b)** Expression of mRNA encoding components of the Hippo pathway (left margin) in various T cell subsets (above plot); two culture replicates per subset (one per column) differentiated from naive CD4⁺ T cells *in vitro*; results were normalized (key) and are presented relative to those of T_{H0} cells, set as 1. **(c)** Immunoblot analysis (top) and real-time quantitative PCR (RT-qPCR) analysis (below) of TAZ expression in various mouse T cell subsets (above lanes (top) and horizontal axis (below)); GAPDH (above) serves as a loading control throughout, and RT-qPCR results are presented relative to those of the internal control gene *Gapdh* throughout. **(d)** Visualization of CD3⁺CD4⁺ T cells from the draining lymph nodes of KLH-treated *Taz^{fl/fl}* and *Taz^{fl/fl}Lck-Cre* mice (above plots) analyzed by mass cytometry (presented as in **a**). **(e)** Flow cytometry (left) and quantification (right) of intracellular IL-17, Foxp3 and IFN- γ in CD4⁺ T cells from the draining lymph nodes (LN) and spleen (left margin (left) and horizontal axis (right)) of KLH-treated *Taz^{fl/fl}* or *Taz^{fl/fl}Lck-Cre* mice ($n = 6$ per genotype). Numbers in quadrants indicate percent cells in each throughout. **(f,g)** RT-qPCR analysis of *TAZ* and *RORC* mRNA (**f**) and correlation of the expression of *TAZ* with that of *RORC* (**g**) in memory CD4⁺ T cells isolated from peripheral blood of healthy donors ($n = 18$) and patients with rheumatoid arthritis (RA; $n = 22$) or Sjögren's syndrome (SS; $n = 21$); results were plotted and analyzed with the linear-regression *t*-test (**g**). **(h)** RT-qPCR analysis of *TAZ* (left) and immunoblot analysis of TAZ (right) in various T cell subsets from healthy human donors (horizontal axis (left) and above lanes (right)). Each symbol (**e–g**) represents an individual mouse (**e**) or donor (**f,g**); small horizontal lines (**e,f**) indicate the mean (\pm s.e.m.). NS, not significant ($P > 0.05$); * $P < 0.05$, ** $P < 0.01$ and *** $P < 0.001$, compared with T_{H0} (**c,h**) or as indicated by bracketing (Student's *t*-test). Data are from one experiment representative of three independent experiments with similar results (**a–e,h**; mean + s.d. of $n = 3$ technical replicates (**c,h**) or $n = 6$ mice per genotype (**e**) or one experiment (**f,g**).

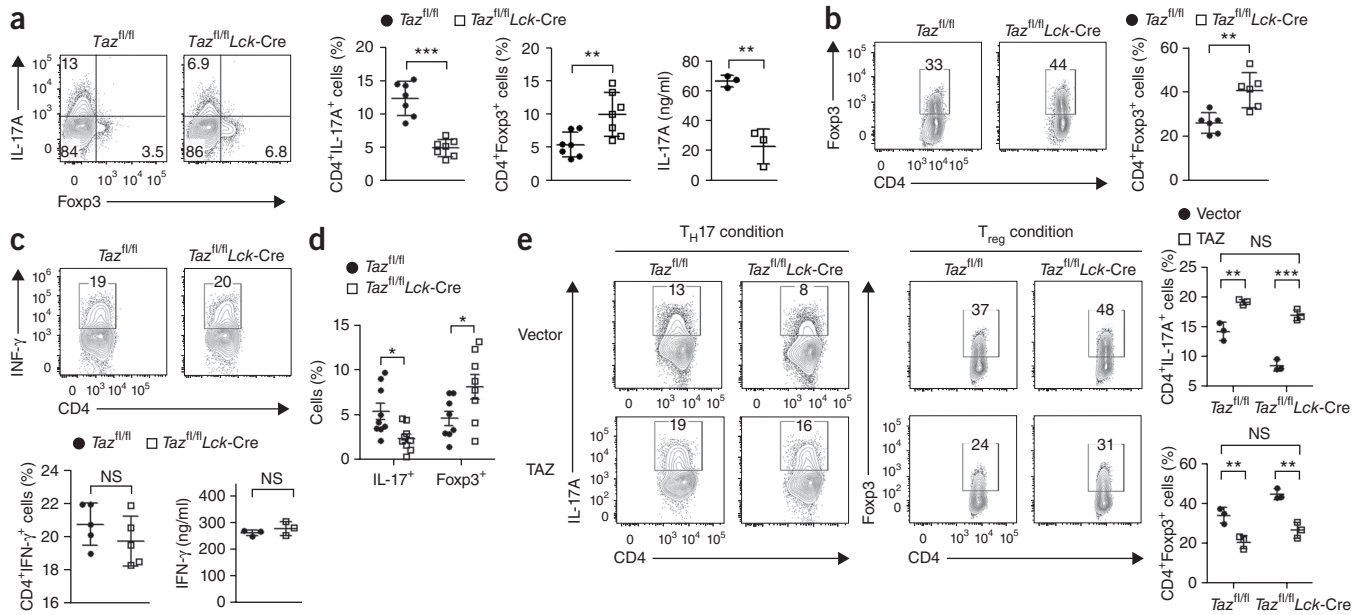


Figure 2 TAZ enhances T_H17 cell differentiation but attenuates T_{reg} cell differentiation *in vitro*. (a–c) Flow cytometry (left (a,b) and top (c)) and quantification (near right (a,b) and bottom left (c)) of intracellular IL-17A, Foxp3 or IFN- γ in naive $CD4^+$ T cells from $Taz^{fl/fl}$ or $Taz^{fl/fl}Lck-Cre$ mice differentiated under T_H17 -polarizing conditions (a), T_{reg} cell-polarizing conditions (b) or T_H1 -polarizing conditions (c), and enzyme-linked immunosorbent assay (ELISA) of IL-17A (a, far right) or IFN- γ (c, bottom right) in the culture medium ($n = 3$ technical replicates). Numbers adjacent to outlined areas indicate percent Foxp3⁺CD4⁺ (T_{reg}) cells (b) or IFN- γ CD4⁺ cells (c). (d) Quantification of CD4⁺IL-17⁺ and CD4⁺Foxp3⁺ cells (horizontal axis) in the colonic LP compartment of naive $Taz^{fl/fl}$ or $Taz^{fl/fl}Lck-Cre$ mice (key). (e) Flow cytometry (top) and quantification (below) of intracellular IL-17A or Foxp3 in $Taz^{fl/fl}$ and $Taz^{fl/fl}Lck-Cre$ naive $CD4^+$ T cells infected with control retrovirus expressing GFP alone (Vector) or retrovirus expressing GFP and TAZ (left margin (top) or key (below)) and differentiated under T_H17 -polarizing conditions (left) or T_{reg} cell-polarizing conditions (right). Numbers adjacent to outlined areas (top) indicate percent IL-17A⁺CD4⁺ (T_H17) cells (left) or Foxp3⁺CD4⁺ (T_{reg}) cells (right). Each symbol represents an individual mouse; small horizontal lines indicate the mean (\pm s.d.). * $P < 0.05$, ** $P < 0.01$ and *** $P < 0.001$, as indicated by bracketing (Student's t -test). Data are representative of three independent experiments with similar results (a–c,e; cell cultures: $n = 7$ (a), $n = 6$ (b), $n = 5$ (c) or $n = 3$ (e) or one experiment with $n = 9$ mice per genotype (d).

wild-type and TAZ-cKO mice with a myelin oligodendrocyte glycoprotein (MOG) peptide of amino acids 35–55 to induce experimental autoimmune encephalomyelitis (EAE). TAZ-deficient mice exhibited a significantly lower incidence and severity of EAE than that of wild-type mice (Fig. 3a). Fewer $CD3^+$ T cells and T_H17 cells infiltrated the central nerve system (CNS) of TAZ-cKO mice than that of wild-type mice at the onset or peak of EAE (Fig. 3b,c and Supplementary Fig. 2k,l). The number of T_{reg} cells was also lower in TAZ-cKO mice than in wild-type mice during EAE, but the ratio of T_{reg} cells to T_H17 cells among cells that infiltrated the CNS was higher in TAZ-cKO mice than in wild-type mice during EAE (Fig. 3b,d). In addition, a lower frequency of $CD4^+$ IL-17⁺ T cells, a higher frequency of $CD4^+$ Foxp3⁺ T cells and a similar frequency of $CD4^+$ IFN- γ ⁺ T cells were present in the draining lymph nodes of TAZ-cKO mice relative to that in wild-type mice (Fig. 3e,f). TAZ-cKO T cells isolated from MOG-immunized mice showed impaired production of IL-17 but normal production of IFN- γ and IL-2 upon restimulation with the MOG peptide noted above (Fig. 3g). Furthermore, TAZ-deficient T_{reg} cells exhibited a much greater ability to suppress the proliferation of naive $CD4^+$ T cells and production of IL-2 than that of wild-type T_{reg} cells (Supplementary Fig. 2m,n). Our result suggested that the TAZ-cKO mice were resistant to EAE owing to a defect in producing T_H17 cells, as well as to enhanced induction and immunosuppressive function T_{reg} cells.

We then obtained naive $CD4^+$ T cells from mice with transgenic T cell-specific expression of *Taz* (TAZ-Tg mice) or TAZ-cKO mice, and from their non-transgenic or non-mutant control littermates, transferred the cells into host mice with a congenital deficiency in mature B cells and T cells (*Rag1*^{-/-} mice) and tracked the development

of colitis, another T_H17 cell-driven autoimmune disorder, in the host mice. Adoptive transfer of TAZ-Tg T cells elicited more-severe weight loss and intestinal inflammation with a significantly greater frequency of T_H17 cells in the colonic LP than that elicited by the transfer of control T cells (Fig. 3h–j). In contrast, host mice reconstituted with TAZ-cKO T cells developed much less severe disease with significantly fewer T_H17 cells in the colon LP than that of mice reconstituted with control T cells (Fig. 3k–m). Consistent with the *in vitro* assay, the development of IFN- γ -producing T_H1 cells was not significantly affected in host mice given transfer of TAZ-Tg or TAZ-cKO T cells (Fig. 3j,m). These results indicated that TAZ probably promoted T cell-mediated colitis by enhancing T_H17 differentiation.

To determine whether autoimmunity induced by MST1 deficiency disease relies on TAZ, we generated mice with double knockout of MST1 and TAZ by crossing *Mst1*^{-/-} mice with *Taz*^{fl/fl}*Lck-Cre* mice (*Mst1*^{-/-}*Taz*^{fl/fl}*Lck-Cre*). *Rag1*^{-/-} mice given adoptive transfer of *Mst1*^{-/-} cells exhibited more severe intestinal inflammation than that of mice that received wild-type (*Taz*^{fl/fl}) cells, while those that received *Mst1*^{-/-}*Taz*^{fl/fl}*Lck-Cre* cells showed less severe signs than those of mice that received wild-type cells (Fig. 3n,o). The frequency of T_H17 cells, but not that of T_H1 cells, was much lower in the LP of mice that received *Mst1*^{-/-}*Taz*^{fl/fl}*Lck-Cre* naive $CD4^+$ T cells than in that of mice that received *Mst1*^{-/-} or wild-type $CD4^+$ T cells (Fig. 3m). Thus, MST1 deficiency resulted in autoimmune disease probably via activation of TAZ.

Smad3 and STAT3 synergistically upregulate *Taz* expression

T_H17 differentiation is initiated by TGF- β and IL-6. We found that the abundance *Taz* mRNA was significantly increased by TGF- β alone

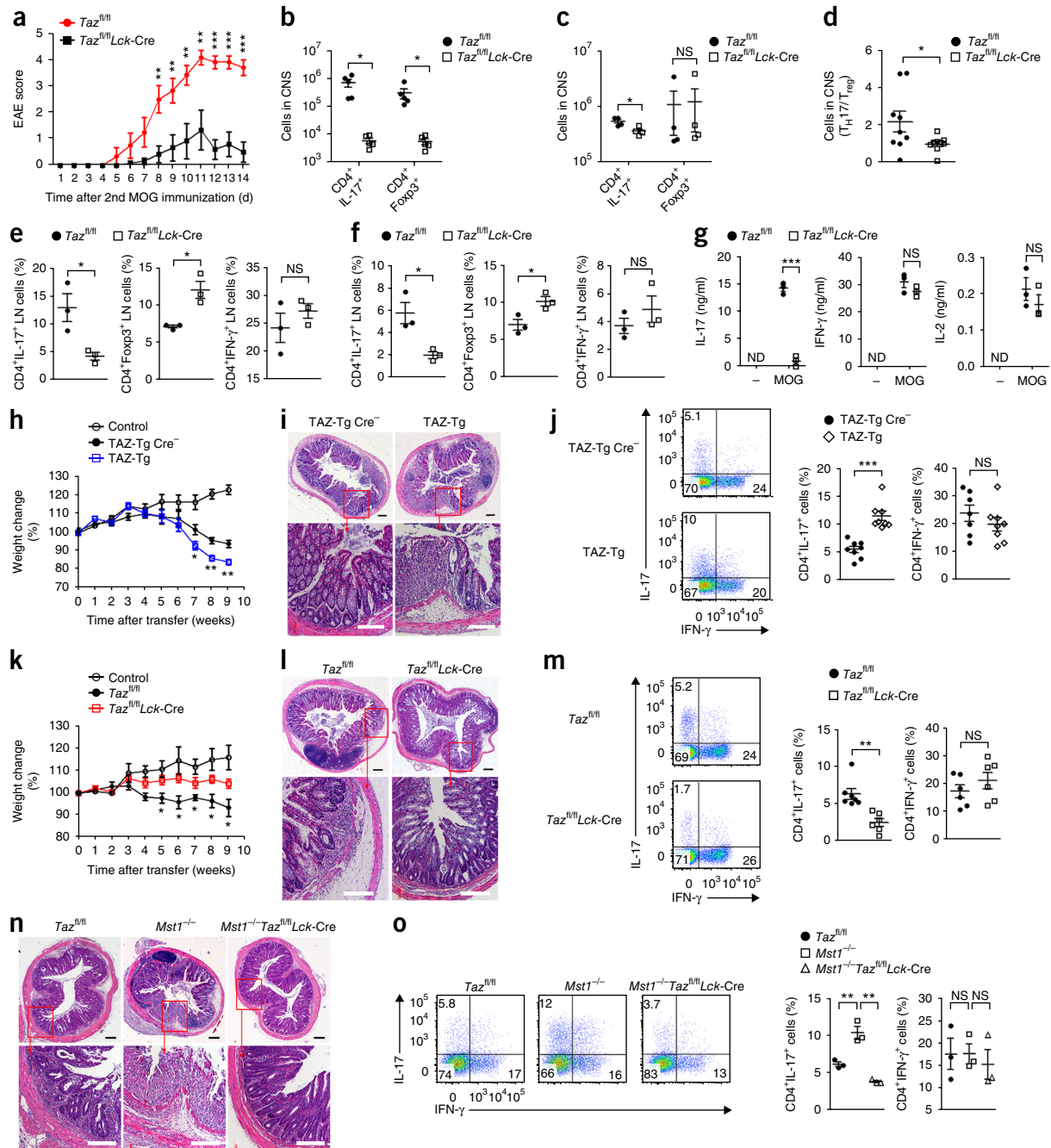


Figure 3 TAZ potentiates T_H17 cell-mediated autoimmune diseases. **(a)** Disease (EAE)-related behavioral scores of $Taz^{fl/fl}$ and $Taz^{fl/fl}Lck-Cre$ mice subjected to MOG-induced EAE ($n = 6$ per genotype). **(b,c)** Quantification (by flow cytometry) of $CD4^+IL-17^+$ and $CD4^+Foxp3^+$ cells that infiltrated the CNS of mice as in **a** at disease onset (**b**; $n = 5$ per genotype) or peak (**c**, $n = 4$ per genotype). **(d)** Ratio of T_H17 cells ($CD4^+IL-17^+$) to T_{reg} cells ($CD4^+Foxp3^+$) in the CNS of mice as in **a**. **(e,f)** $CD4^+IL-17^+$, $CD4^+Foxp3^+$ or $CD4^+IFN-\gamma^+$ cells in the draining lymph nodes of mice as in **a** at disease onset (**e**; $n = 3$ per genotype) or peak (**f**; $n = 3$ per genotype). **(g)** ELISA of IL-17, IFN- γ and IL-2 in supernatants of cells obtained from the draining lymph nodes of mice as in **a** and left unstimulated (-) or stimulated for 2 d *in vitro* with MOG ($n = 3$ technical replicates). **(h,k)** Body weight of $Rag1^{-/-}$ recipient mice at various times (horizontal axes) after adoptive transfer (key) of no cells (Control) or 4×10^5 TAZ-Tg $Cre^{-/-}$ or TAZ-Tg naive $CD4^+$ T cells (**h**; $n = 7$ host mice per group) or 4×10^5 $Taz^{fl/fl}$ or $Taz^{fl/fl}Lck-Cre$ naive $CD4^+$ T cells (**k**; $n = 5$ host mice per group), presented relative to initial body weight. **(i,l)** Microscopy of hematoxylin-and-eosin-stained colon sections of mice as in **h** (**i**) or **k** (**l**) at 9 weeks after cell transfer (above images); bottom row, enlargement of areas outlined in main images above. Scale bars, 200 μm . **(j,m)** Flow cytometry (left) and quantification (right) of $CD4^+IL-17^+$ and $CD4^+IFN-\gamma^+$ cells in the colonic LP of mice given transfer of donor cells (left margin (left) or key (right)) as in **i** (**j**; $n = 8$ host mice per group) or **l** (**m**; $n = 6$ host mice per group). **(n)** Microscopy of hematoxylin-and-eosin-stained colon sections from $Rag1^{-/-}$ recipient mice after adoptive transfer of 4×10^5 $Taz^{fl/fl}$, $Mst1^{-/-}$ or $Mst1^{-/-}Taz^{fl/fl}Lck-Cre$ naive $CD4^+$ T cells (above images). Scale bars, 200 μm . **(o)** Flow cytometry (left) and quantification (right) of $CD4^+IL-17^+$ and $CD4^+IFN-\gamma^+$ cells in the colonic LP of mice as in **n** ($n = 3$ per group). ND, not detectable. Each symbol (**b-g,j,m,o**) represents an individual mouse; small horizontal lines indicate the mean (\pm s.e.m.). * $P < 0.05$, ** $P < 0.01$ and *** $P < 0.001$, $Taz^{fl/fl}$ versus $Taz^{fl/fl}Lck-Cre$ (**a,k**) or TAZ-Tg $Cre^{-/-}$ versus TAZ-Tg (**h**) or as indicated by bracketing (Student's t -test). Data are representative of three independent experiments with similar results (mean \pm s.e.m. in **a,h,k**).

but not by IL-6 alone and that this increase was further enhanced by stimulation with a combination of TGF- β and IL-6 (Fig. 4a–c). Furthermore, treatment with an inhibitor of the TGF- β receptor TGF- β R2 resulted in a reduction in the expression of *Taz* mRNA in a dose-dependent manner (Fig. 4d), which indicated that TGF- β was an essential factor in the induction of *Taz* expression.

To identify transcription factors that control *Taz* expression, we generated 2-kb biotinylated DNA fragments corresponding to *Taz* promoter sequences upstream of the ATG start codon and incubated them with mouse lymphoid tissue lysates, followed by a streptavidin-precipitation assay. Several potential transcriptional factors, including Smad3 and STAT3 (the main transcription factor downstream of signaling via TGF- β or IL-6), were identified by mass spectrometry (Supplementary Fig. 3). We found that knockdown of Smad3 or knockout of STAT3 significantly decreased TAZ expression in HeLa human cervical cancer cells or naive CD4⁺ T cells cultured under T_H17-skewing conditions (Fig. 4e–g). Conversely, overexpression of Smad3 resulted in the induction of TAZ expression, and co-expression Smad3 with STAT3 further enhanced the TAZ expression (Fig. 4h,i). In addition, there are ten known Smad-binding sequences (GAG(A/C)C, where '(A/C)' indicates either adenosine or cytosine) and ten STAT-binding sequences (TT(N₅)AA, where '(N₅)' indicates five nucleotides of any type) in the 2-kb region of the *Taz* promoter (Fig. 4j). Consistent with that, Smad3 increased the activity of the *Taz* promoter, but STAT3 did not, while Smad3 together with STAT3 synergistically enhanced this activity (Fig. 4k). Since the 1-kb and 2-kb *Taz* promoter regions have comparable activity, the essential binding sites of Smad3 or STAT3 for the transcription of *Taz* were probably located within the 1-kb promoter region. Direct binding of Smad3 and STAT3 to the 1-kb promoter region was further confirmed by streptavidin-precipitation and chromatin-immunoprecipitation assays (Fig. 4l–n). Moreover, we measured and compared the activity of a luciferase reporter containing the *Taz* 1-kb promoter with individual mutated Smad-binding and/or STAT3-binding sites. We found that a Smad-binding site in the region –225 bp to –192 bp and a STAT3-binding site in the region of –282 bp to –240 bp (all positions relative to the transcription start site) were critical for *Taz* expression (Fig. 4o). Thus, we concluded that TGF- β –IL-6 signaling promoted *Taz* expression through the downstream transcription factors Smad3 and STAT3.

TAZ directly activates ROR γ t's transcriptional activity

We next sought to delineate the molecular mechanism underlying the promotion of T_H17 cell development by TAZ. For this, we used anti-Flag beads to immunoprecipitate proteins from lysates of lymphoid tissues from wild-type or TAZ-Tg mice in which Flag-tagged TAZ was overexpressed, then further analyzed the resultant immunoprecipitates by mass spectrometry. Notably, the components identified included known binding proteins of the TEAD family, as well as previously unknown binding partners, such as ROR γ t, Foxp3, Tip60 and others (Supplementary Fig. 4a). Furthermore, endogenous ROR γ t and Foxp3 were co-immunoprecipitated with TAZ in mixed lysates of T_H17 cells and T_{reg} cells (Supplementary Fig. 4b). To map the interaction regions of TAZ and ROR γ t, we expressed green fluorescent protein (GFP)-tagged ROR γ t with a series of Flag-tagged truncated forms of TAZ, or vice versa, in 293T human embryonic kidney cells, followed by precipitation assays (Fig. 5a–d and Supplementary Fig. 4c,d). We found that the tryptophan-tryptophan (WW) domain of TAZ was essential for its interaction with ROR γ t, whereas the DNA-binding domain (DBD) and ligand-binding domain (LBD) of ROR γ t were responsible for its interaction with TAZ (Fig. 5e). The TAZ–ROR γ t

interaction in the nucleus was further analyzed by a super-resolution immunofluorescence microscopy (SIM) approach. Notably, nuclear-localization sequence (NLS)-tagged TAZ alone formed circular foci (probably a polymer of TAZ aggregates) in the nucleus, whereas full-length or truncated fragments of ROR γ t alone were evenly distributed in the nucleus (Supplementary Fig. 4e). Consistent with the biochemical data, full-length ROR γ t and its DBD or LBD, but not its hinge portion, localized together with TAZ and formed circular foci (Fig. 5f). These data demonstrated that TAZ physically bound to ROR γ t *in vitro* and *in vivo*.

Moreover, the WW domain of TAZ interacted with the LBD of ROR γ t via the WW-domain-binding motif PPxY (Pro-Pro-x-Tyr, where 'x' indicates any amino acid) located in the carboxy-terminal activation-function region AF2 of ROR γ t. Mutant ROR γ t in which the amino acids Pro-Pro-Leu-Tyr of AF2 were replaced with Ala-Pro-Leu-Ala failed to bind to TAZ (Fig. 5f,g). Since AF2 is the main transcription-activation motif of ROR γ t, we speculated that TAZ might act as a co-activator of ROR γ t for the transcription of *Il17a*. Indeed, wild-type TAZ increased ROR γ t-mediated activity of the *Il17a* promoter in a dose-dependent manner, but a truncated form of TAZ lacking the WW domain, which was unable to interact with ROR γ t, did not (Fig. 5h,i). Consistent with that, overexpression of wild-type TAZ in naive CD4⁺ T cells resulted in a significantly higher frequency of IL-17⁺ cells under T_H17-skewing conditions, but overexpression of the truncated form of TAZ lacking the WW domain did not (Fig. 5j). Moreover, overexpression of TAZ in ROR γ t-deficient naive CD4⁺ T cells was unable to induce T_H17 differentiation (Fig. 5k), which indicated that ROR γ t was required for the TAZ-mediated development of T_H17 cells. These results suggested that TAZ was a critical co-activator of ROR γ t for T_H17 differentiation.

TAZ blocks T_{reg} cell differentiation by inhibiting Foxp3

The developmental pathway for T_H17 cells and that for T_{reg} cells are reciprocally interconnected⁸. Notably, TAZ deficiency resulted in increased production of Foxp3 in T cells under both T_H17-skewing conditions and T_{reg} cell-skewing conditions (Fig. 6a). However, the abundance of *Foxp3* mRNA was comparable in wild-type cells and TAZ-deficient cells (Supplementary Fig. 5a), which indicated that TAZ might regulate the stability of Foxp3 protein. Indeed, TAZ promoted the degradation of Foxp3 protein, which was blocked by the proteasome inhibitor MG132 (Fig. 6b,c).

The acetylation of Foxp3 by the histone acetyltransferases Tip60 and p300 is essential for inhibiting proteasomal degradation of Foxp3 (ref. 43). Notably, TAZ-deficient T_{reg} cells exhibited greater acetylation but less ubiquitination of endogenous Foxp3 than that of wild-type cells (Fig. 6d). Conversely, overexpression of TAZ attenuated the effect of Tip60 and p300 on the acetylation and stabilization of Foxp3 (Fig. 6e,f). In addition, we found that the coiled-coil domain of TAZ (residues 158–249) interacted with the zinc domain of Tip60 (residues 113–283), while Foxp3 bound to the zinc-and-acetyltransferase-MYST domain of Tip60 (residues 113–513) (Supplementary Fig. 5b–d). These results suggested that TAZ might compete with Foxp3 to bind to the same motif between residues 113 and 283 of Tip60 (Fig. 6g). Indeed, co-immunoprecipitation assays showed that TAZ exhibited higher affinity for Tip60 and efficiently disrupted the interaction between Tip60 and Foxp3 (Fig. 6h,i and Supplementary Fig. 5e). SIM further confirmed that the interaction of Foxp3 and Tip60 was abolished by TAZ (Fig. 6j and Supplementary Fig. 5f). Together these data indicated that TAZ impaired T_{reg} cell development probably by sequestering Tip60 from Foxp3 and diminishing the Tip60-mediated acetylation of Foxp3 and targeting it for proteasomal degradation.

TAZ activates ROR γ t by blocking Foxp3 activity

The data reported above established that TAZ negatively regulated the stability of Foxp3. We found that both ROR γ t and Foxp3 immunoprecipitated together with TAZ (Supplementary Fig. 4a) and that the

WW domain of TAZ was critical for its binding to ROR γ t (Fig. 5e). In addition, the WW domain of TAZ and the domain of Foxp3 consisting of amino acids 190–280 were essential for their interaction (Fig. 7a and Supplementary Fig. 6a–d). The LxxLL (Leu-x-x-Leu-Leu) motif

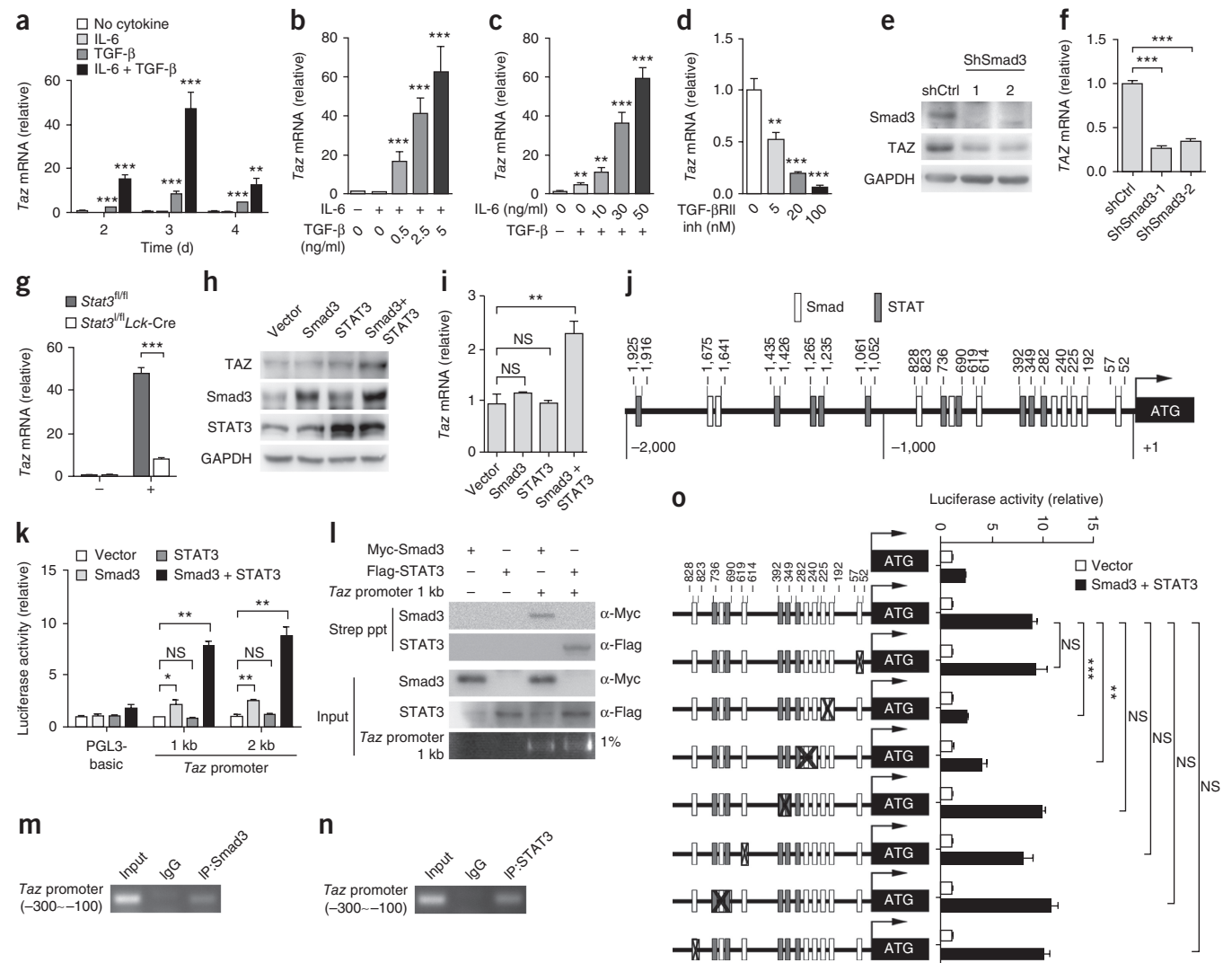


Figure 4 Smad proteins and STAT3 synergistically upregulate TAZ expression. (a–c) RT-qPCR analysis of *Taz* mRNA in naive CD4⁺ T cells cultured for 2, 3 or 4 d (horizontal axis) with anti-CD3 plus anti-CD28 alone (No cytokine) or together with TGF- β (2.5 ng/ml) or IL-6 (30 ng/ml) or both (key) (a) or for 3 d with anti-CD3 plus anti-CD28 together with a combination of IL-6 (+) or not (–) and various concentrations (below plot) of TGF- β (b) or TGF- β (+) or not (–) and various concentrations (below plot) of IL-6 (c); results are presented relative to those of *Gapdh*. (d) RT-qPCR analysis of *Taz* mRNA in naive CD4⁺ T cells cultured for 3 d as in a with various concentrations (below plot) of the TGF- β RII inhibitor (inh); results presented as in a–c. (e,f) Immunoblot analysis of Smad3 and TAZ (e) and RT-qPCR analysis of *TAZ* mRNA (f) in HeLa cells treated with control (non-targeting) short hairpin RNA (shRNA) (shCtrl) or either of two shRNAs (1, 2) targeting Smad3 (shSmad3); RT-qPCR results are presented relative to those of *GAPDH*. (g) RT-qPCR analysis of *Taz* mRNA in *Stat3*^{fl/fl} or *Stat3*^{fl/fl}*Lck-Cre* naive CD4⁺ T cells (key) cultured for 3 d with anti-CD3 plus anti-CD28 without cytokines (–) or together with TGF- β (2.5 ng/ml) and IL-6 (30 ng/ml) (+). (h,i) Immunoblot analysis of TAZ, Smad3 and STAT3 (h) and RT-qPCR analysis of *Taz* mRNA (i) in naive CD4⁺ T cells infected with retrovirus expressing GFP alone (Vector) or GFP plus Smad3 or STAT3 or both (above lanes (h) or horizontal axis (i)). (j) Smad- and STAT-binding sites (key) in the *Taz* promoter region; numbers above diagram indicate position relative to the transcription start site (ATG; far right), and those below (with vertical lines) demarcate the 1-kb and 2-kb promoter regions. (k) Luciferase activity of 293T cells transfected with an empty luciferase reporter construct (pGL3-basic) or a construct containing the 1-kb or 2-kb *Taz* promoter (horizontal axis) and retrovirus as in h,i (key); firefly luciferase activity was normalized to that of *Renilla*, and results are presented relative to those of cells transfected with the empty luciferase construct and empty retroviral vector. (l) Streptavidin-precipitation (Strep ppt) assay (top) of 293T cells expressing various combinations (above lanes) of Myc-tagged Smad3 or Flag-tagged STAT3 and a biotinylated 1-kb *Taz* promoter, probed with anti-Myc (α -Myc) or anti-Flag (α -Flag) (right margin); below, input of total chromatin fragments (1% agarose (bottom) indicates *Taz* promoter DNA). (m,n) Chromatin immunoprecipitation of T_H17 cells with the control antibody IgG or anti-Smad3 (m) or anti-STAT3 (n), followed by PCR with primers covering the Smad3- or STAT3-binding sequences from position –300 to position –100 of the *Taz* promoter; Input (far left lane), PCR as above without immunoprecipitation. (o) Luciferase activity (assessed as in k) of 293T cells transfected with empty vector or plasmids expressing Smad3 and STAT3 (key) and with a luciferase reporter containing the 1-kb *Taz* promoter (left margin) with or without various deletions ('X'). * $P < 0.05$, ** $P < 0.01$ and *** $P < 0.001$, compared with cells cultured without cytokines or as indicated by bracketing (Student's *t*-test). Data are representative of three independent experiments with similar results (mean + s.d. in a–d,f,g,i,k,o).

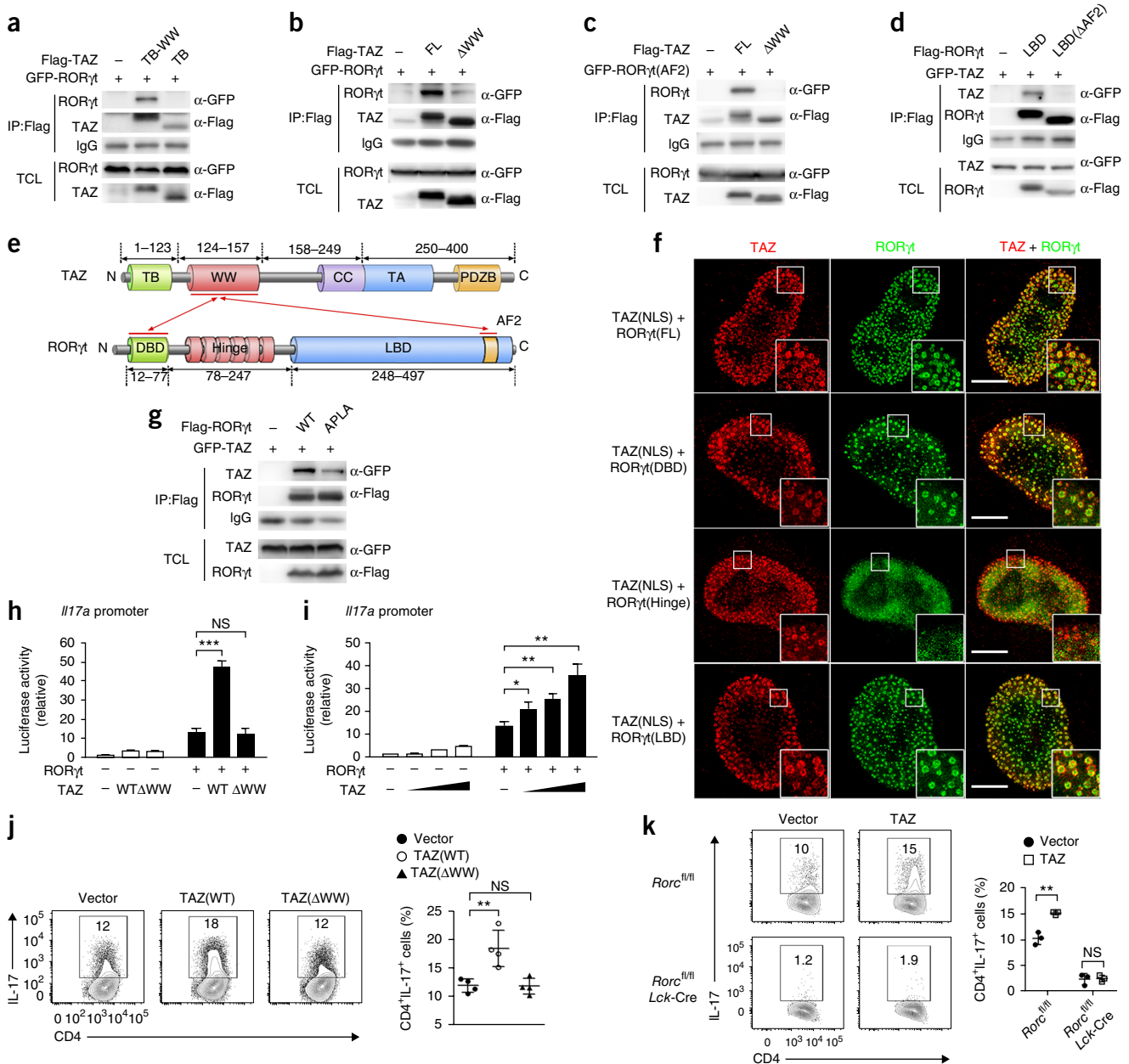


Figure 5 TAZ binds to ROR γ t and enhances its transcriptional activity. **(a–d)** Immunoblot analysis of ROR γ t and various forms of TAZ (above lanes) in total cell lysates (TCL; bottom) and anti-Flag immunoprecipitates (IP: Flag) (above) of 293T cells expressing GFP-tagged ROR γ t (+) (above lanes) alone (–) or together with Flag-tagged TEAD-binding domain with (TB-WW) or without (TB) the WW domain **(a)** or full-length TAZ (FL) or TAZ lacking the WW domain (Δ WW) **(b)**, expressing a GFP-tagged AF2 fragment of ROR γ t (GFP-ROR γ t(AF2)) (+) (above lanes) alone (–) or together with full-length TAZ or TAZ lacking the WW domain **(c)**, or expressing GFP-tagged TAZ (+) (above lanes) alone (–) or together with the LBD of ROR γ t or that LBD with deletion of AF2 (LBD(Δ AF2)) **(d)**, probed with anti-GFP or anti-Flag (right margin). **(e)** Interaction between TAZ and ROR γ t, showing the domains involved (red arrows); numbers above and below diagrams indicate amino acid range of each domain. CC, coiled-coil domain; TA, transcription-activation domain; PDZB, PDZ-binding domain. **(f)** SIM of HeLa cells cotransfected to express NLS- and Flag-tagged TAZ (TAZ(NLS)) (red) with full-length ROR γ t (ROR γ t(FL)) or the DBD, Hinge domain or LBD of ROR γ t (green) (left margin); insets (bottom right corners), 4 \times enlargement of areas outlined in main images. Scale bars, 20 μ m. **(g)** Immunoprecipitation assay (as in **a**) of 293T cells expressing GFP-tagged TAZ alone (+) (above lanes) (–) or together with Flag-tagged wild-type ROR γ t (WT) or ROR γ t with Pro-Pro-Leu-Tyr of AF2 replaced with Ala-Pro-Leu-Ala (APLA). **(h,i)** Luciferase activity of 293T cells transfected with a luciferase reporter driven by the *Il17a* promoter plus various combinations (below plots) of expression plasmids for ROR γ t and wild-type TAZ (WT) or TAZ lacking the WW domain (Δ WW) **(h)** or various doses (wedges) of expression plasmid for wild-type TAZ **(i)** (results presented as in **Fig. 4k**). **(j,k)** Flow cytometry (left) and quantification (right) of intracellular IL-17 in naive CD4⁺ T cells infected with control retrovirus (Vector) or retrovirus expressing wild-type TAZ or TAZ lacking the WW domain (above plots (left) or horizontal axis (right)) **(j)** or in *Rorc*^{fl/fl} and *Rorc*^{fl/fl}Lck-Cre naive CD4⁺ T cells (left margin (left) or key (right)) infected with control retrovirus (Vector) or retrovirus expressing wild-type TAZ (above plots (left) or horizontal axis (right)) **(k)**, differentiated under T_H17-polarizing conditions. Numbers in outlined areas (left) indicate percent IL-17⁺CD4⁺ (T_H17) cells. Each symbol **(j,k)** represents an individual cell culture; small horizontal lines indicate the mean (\pm s.d.). * $P < 0.05$, ** $P < 0.01$ and *** $P < 0.001$, as indicated by bracketing (Student's *t*-test). Data are representative of three independent experiments with similar results **(a–d,g–k)**; mean \pm s.d. of $n = 3$ technical replicates **(h,i)**, or $n = 4$ **(j)** or $n = 3$ **(k)** cell cultures) or with ~ 50 cells **(f)**.

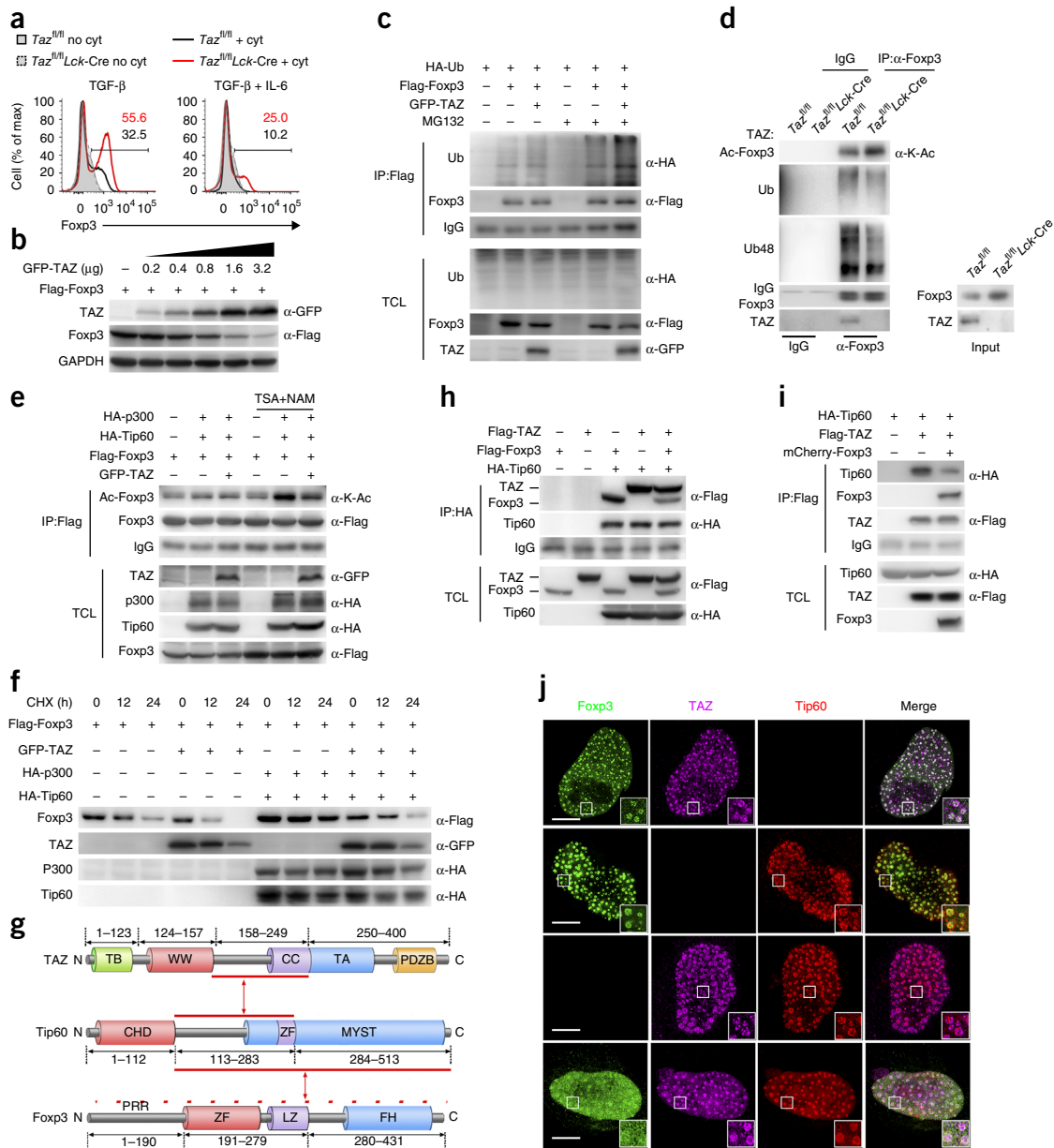


Figure 6 TAZ blocks the acetylation of Foxp3 and promotes its degradation. **(a)** Flow cytometry analyzing Foxp3 in $Taz^{fl/fl}$ and $Taz^{fl/fl}Lck-Cre$ naive CD4⁺ T cells (key) without cytokines (no cyt) or under T_{reg} cell-polarizing conditions (+ cyt) (left) or T_H17 -polarizing conditions (+ cyt) (right). Numbers above bracketed lines indicate percent Foxp3⁺ cells (font color matches key). **(b)** Immunoblot analysis of TAZ and Foxp3 in 293T cells expressing Flag-tagged Foxp3 and increasing doses (wedge; concentrations above lanes) of GFP-tagged TAZ. **(c)** Immunoblot analysis of the ubiquitination (Ub) of Foxp3 in 293T cells expressing various combinations (above lanes) of hemagglutinin-tagged ubiquitin (HA-Ub), Flag-tagged Foxp3 and GFP-tagged TAZ and treated with the vehicle DMSO (-) or the proteasome inhibitor MG132 (+), assessed anti-Flag immunoprecipitates (top group) or total cell lysates (below), probed with various antibodies (right margin). **(d)** Immunoblot analysis of the acetylation (Ac) and ubiquitination (Ub) of Foxp3 in T_{reg} cells differentiated from $Taz^{fl/fl}$ or $Taz^{fl/fl}Lck-Cre$ naive CD4⁺ T cells (above lanes), assessed in lysates after immunoprecipitation with the control antibody IgG or anti-Foxp3 (below blots); right, immunoblot analysis of total cell lysates without immunoprecipitation. α -K-Ac, antibody to acetylated lysine; Ub48, Lys48-linked ubiquitination. **(e)** Immunoassay of 293T cells expressing various combinations (above lanes) of HA-tagged Tip60 and p300, Flag-tagged Foxp3 and GFP-tagged TAZ and treated with DMSO (-) or the histone-deacetylase inhibitors (+) trichostatin A and nicotinamide (TSA&NAM), assessed in anti-Flag immunoprecipitates (top group) or total cell lysates (below), probed with various antibodies (right margin). **(f)** Immunoblot analysis of lysates of 293T cells expressing various combinations (above lanes) of Flag-tagged Foxp3, GFP-tagged TAZ and HA-tagged p300 and Tip60 and treated for various times (above lanes) with DMSO (0) or the protein-synthesis inhibitor cycloheximide (CHX), probed with various antibodies (right margin). **(g)** Interaction between Tip60 and TAZ or between Tip60 and Foxp3, showing the domains involved (red arrows; red dots indicate domain involvement not yet identified); numbers above and below diagrams indicate amino acid range of each domain. CHD, chromodomain; ZF, zinc-finger domain; MYST, histone acetyltransferase domain; PRR, proline-rich region; LZ, leucine zipper domain; FH, forkhead domain. **(h,i)** Immunoassay of 293T cells expressing various combinations (above lanes) of Flag-tagged TAZ, Flag-tagged Foxp3 and HA-tagged Tip60 (**h**) or HA-tagged Tip60, Flag-tagged TAZ and mCherry-tagged Foxp3 (**i**), assessed in lysates after immunoprecipitation with anti-HA (**h**) or anti-Flag (**i**) (top group) or in total cell lysates without immunoprecipitation (below), probed with anti-HA or anti-Flag. **(j)** SIM of HeLa cells cotransfected to express various combinations of NLS- and Flag-tagged TAZ (purple), GFP-tagged Foxp3 (green) and HA-tagged Tip60 (red) (insets as in **Fig. 5f**). Scale bars, 20 μ m. Data are representative of three independent experiments with similar results (**a-f**) or with ~50 cells (**j**) or three experiments (**h,i**).

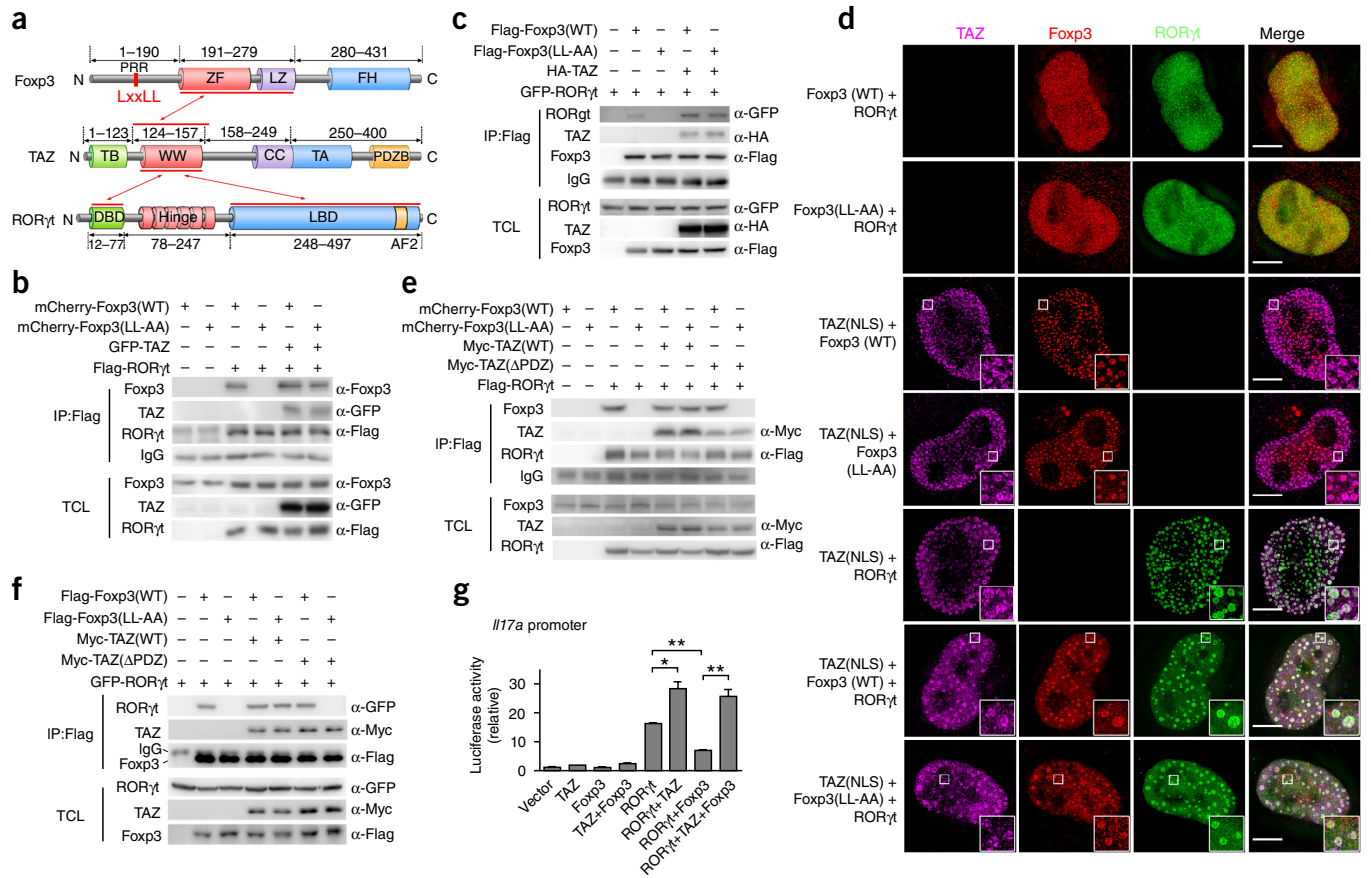


Figure 7 TAZ activates RORγt by blocking the inhibitory effect of Foxp3 on RORγt. **(a)** Interaction between Foxp3 and TAZ or between RORγt and TAZ, showing the domains involved (red arrows) and the Leu-x-x-Leu-Leu motif (LxxLL; top left); numbers above and below diagrams indicate amino acid range of each domain. **(b)** Immunoassay of 293T cells expressing various combinations (above lanes) of mCherry-tagged wild-type Foxp3 or Foxp3(LL-AA), GFP-tagged TAZ and Flag-tagged RORγt, assessed anti-Flag immunoprecipitates (top group) or total cell lysates (below), probed with various antibodies (right margin). **(c)** Immunoassay (as in **b**) of 293T cells expressing various combinations of Flag-tagged wild-type Foxp3 or Foxp3(LL-AA), HA-tagged TAZ and GFP-tagged RORγt. **(d)** SIM of HeLa cells cotransfected to express (left margin) NLS- and Flag-tagged TAZ (purple), mCherry-tagged wild-type Foxp3 or Foxp3(LL-AA) (red) or GFP-tagged RORγt (green) (insets as in **Fig. 5f**). Scale bars, 20 μm. **(e, f)** Immunoassay (as in **b**) of 293T cells expressing various combinations (above lanes) of mCherry-tagged **(e)** or Flag-tagged **(f)** wild-type Foxp3 or Foxp3(LL-AA), Myc-tagged wild-type TAZ or truncated TAZ lacking the PDZ-binding motif (TAZ(ΔPDZ)), and Flag-tagged RORγt **(e)** or GFP-tagged RORγt **(f)**. **(g)** Luciferase activity of 293T cells transfected with a luciferase reporter driven by the *Il17a* promoter and expressing vector alone (far left) or various combinations (horizontal axis) of TAZ, Foxp3 and RORγt (results presented as in **Fig. 4k**). * $P < 0.01$ and ** $P < 0.001$ (Student's *t*-test). Data are representative of three independent experiments with similar results (**b–f**) or with ~50 cells **(d)** or three experiments **(g)**; mean + s.d. of $n = 3$ technical replicates.

located between residues 90 and 100 of Foxp3 is responsible for its interaction with RORγt⁴³. RORγt failed to bind to a mutant Foxp3 in which the amino acid pair Leu-Leu in that motif was replaced with Ala-Ala (Foxp3(LL-AA)) (**Fig. 7b,c**). Those findings indicated that TAZ and RORγt bound to distinct regions of Foxp3, while Foxp3 and RORγt bound to the same site: the WW domain of TAZ. Notably, co-immunoprecipitation assays showed that Foxp3, RORγt and TAZ were able to form a complex (**Fig. 7b,c** and **Supplementary Fig. 6d**), which indicated that Foxp3 did not compete with RORγt for binding to TAZ. Moreover, in the presence of TAZ, RORγt was able to co-precipitate wild-type Foxp3 and the mutant Foxp3(LL-AA) that was unable to bind to RORγt (**Fig. 7b**). Conversely, either wild-type Foxp3 or Foxp3(LL-AA) was able to co-precipitate RORγt in the presence of TAZ (**Fig. 7c**), which indicated that TAZ might function as a scaffold to promote assembly of the Foxp3–TAZ–RORγt complex. Furthermore, SIM confirmed our findings (**Fig. 7d** and **Supplementary Fig. 6e**). These data suggested that TAZ might form a dimer or polymer to recruit Foxp3 and RORγt. TAZ polymerizes and forms foci through its motif for binding PDZ scaffolding structural domains¹⁰.

Indeed, a truncated form of TAZ lacking the PDZ-binding motif impaired formation of the Foxp3(LL-AA)–TAZ–RORγt complex (**Fig. 7e,f**), which indicated that dimerized or polymerized TAZ was essential for assembly of the Foxp3–TAZ–RORγt complex (**Supplementary Fig. 6f**). Since Foxp3 can inhibit T_H17 differentiation by antagonizing the function of RORγt⁴, we speculated that TAZ might block the inhibitory effect of Foxp3 on RORγt. Indeed, co-expression of TAZ with Foxp3 and RORγt efficiently blocked the inhibitory effect of Foxp3 on RORγt activity (**Fig. 7g**). Together these results demonstrated that TAZ, RORγt and Foxp3 formed a complex in which TAZ blocked the inhibitory effect of Foxp3 on RORγt.

TEAD sequesters TAZ and inhibits T_H17 development

MST1 and MST2 phosphorylate and activate the kinases LATS1 and LATS2, which phosphorylate TAZ at Ser89; this results in its retention in the cytoplasm or proteasome-mediated degradation⁴⁴. Once Hippo signaling is inactivated, dephosphorylated TAZ translocates into the nucleus, where it binds to TEAD via residue Ser51 (of TAZ) and activates TEAD⁴⁵. Notably, overexpression of either

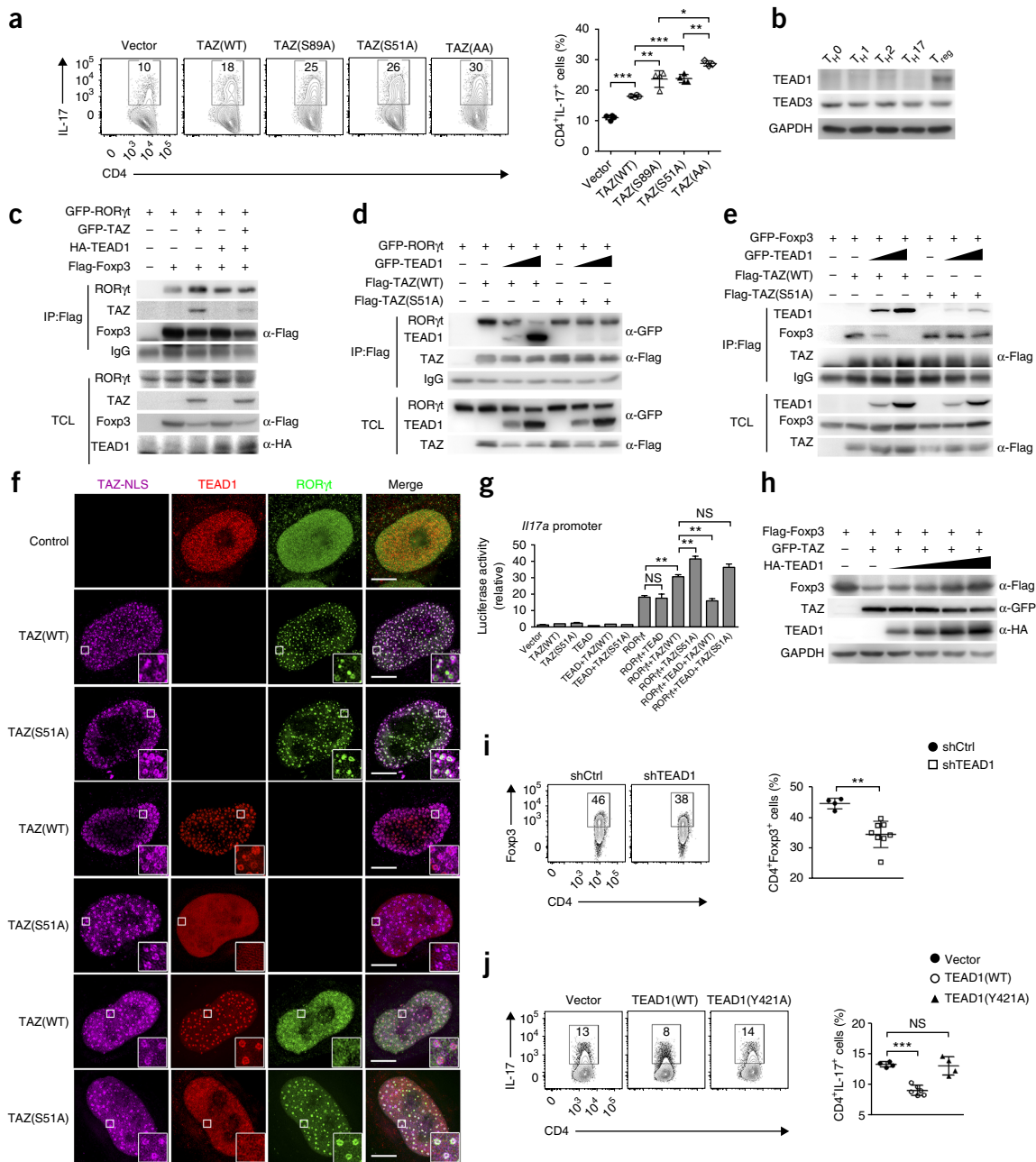


Figure 8 TEAD sequesters TAZ from ROR γ t to promote T_{reg} cell development. **(a)** Flow cytometry (left) and quantification (right) of intracellular IL-17 in wild-type naive CD4⁺ T cells infected with empty retrovirus (Vector) or retrovirus expressing wild-type TAZ(WT), TAZ(S89A), TAZ(S51A) or TAZ(AA) (both substitutions) and differentiated under T_H17-polarizing conditions. Numbers adjacent to outlined areas (left) indicate percent IL-17⁺CD4⁺ (T_H17) cells. **(b)** Immunoblot analysis of TEAD1 or TEAD3 in total lysates of various T cell subsets (above lanes). **(c)** Immunoassay of 293T cells expressing various combinations (above lanes) of GFP-tagged ROR γ t or TAZ, HA-tagged TEAD and Flag-tagged Fopx3, assessed anti-Flag immunoprecipitates (top group) or total cell lysates (below), probed with various antibodies (right margin). **(d,e)** Immunoassay (as in **(c)**) of 293T cells expressing various combinations (above lanes) of GFP-tagged ROR γ t **(d)** or GFP-tagged Fopx3 **(e)** plus increasing doses (wedges) of GFP-tagged TEAD1, and Flag-tagged wild-type TAZ or TAZ(S51A). **(f)** SIM of HeLa cells with no expression of TAZ (Control) or cotransfected to express (left margin) NLS- and Flag-tagged wild-type TAZ or TAZ(S51A) (purple), HA-tagged TEAD1 (red) or GFP-tagged ROR γ t (green) (insets as in **Fig. 5f**). Scale bars, 20 μ m. **(g)** Luciferase activity of 293T cells transfected with a luciferase reporter driven by the *I17a* promoter and expressing empty vector (far left) or various combinations (horizontal axis) of wild-type TAZ, TAZ(S51A), TEAD1 and ROR γ t (results presented as in **Fig. 4k**). **(h)** Immunoblot analysis of Fopx3, TAZ and TEAD1 in total lysates of 293T cells expressing various combinations (above lanes) of Flag-tagged Fopx3, GFP-tagged TAZ and increasing doses (wedge) of HA-tagged TEAD1. **(i,j)** Flow cytometry (left) and quantification (right) of Fopx3 in wild-type naive CD4⁺ T cells infected with a retrovirus expressing control shRNA (shCtrl) or shRNA targeting TEAD1 (shTEAD1) (above plots (left) or key (right)), differentiated under T_{reg} cell-polarizing conditions **(i)**, or of intracellular IL-17 in wild-type naive CD4⁺ T cells infected with empty retrovirus (Vector) or retrovirus expressing wild-type TEAD1 (WT) or TAZ-unbound TEAD1 (TEAD1(Y421A)) (above plots (left) or key (right)), differentiated under T_H17-polarizing conditions **(j)**. Numbers in outlined areas (left) indicate percent Fopx3⁺CD4⁺ (T_{reg}) cells **(i)** or IL-17⁺CD4⁺ (T_H17) cells **(j)**. Each symbol **(a,i,j)** represents an individual cell culture; small horizontal lines indicate the mean (\pm s.d.). * P < 0.05, ** P < 0.01 and *** P < 0.001, as indicated by bracketing (Student's *t*-test). Data are representative of three independent experiments with similar results **(a-d,f-j; n = 4 cell cultures (a), n = 3 technical replicates (f), n = 4 (shCtrl) or 7 (shTEAD1) cell cultures (i) or n = 4 (Vector), 6 (WT) 4 (Y421A) cell cultures (j); error bars (g), s.d.) or with ~50 cells (e).**

a Hippo-refractory and active TAZ mutant, in which the serine at position 89 was replaced with alanine (TAZ(S89A)), or a TEAD-binding-deficient TAZ mutant, in which the serine at position 51 was replaced with alanine (TAZ(S51A)), significantly enhanced the induction of T_H17 cells, and overexpression of a TAZ mutant with both substitutions induced a significantly greater frequency of IL-17A⁺ cells than did overexpression of any other form of TAZ (Fig. 8a). These data indicated that both activation of Hippo signaling and the presence of TEAD proteins negatively regulated TAZ-mediated T_H17 differentiation. Notably, expression of TEAD1, TEAD2 and TEAD4 was undetectable and expression of TEAD3 remained unchanged under T_{reg} cell- or T_H17-skewing conditions, while expression of TEAD1 was robustly induced under T_{reg} cell-skewing conditions (Fig. 8b). Immunoprecipitation assays showed that TEAD1 had a higher affinity for TAZ than that of RORγt or Foxp3 and was able to disrupt the interaction of TAZ with RORγt or Foxp3 (Fig. 8c–e and Supplementary Fig. 7a,b). SIM further confirmed those findings (Fig. 8f and Supplementary Fig. 7c). Moreover, TEAD1 significantly decreased the TAZ- or RORγt-mediated activity of the *Il17a* promoter (Fig. 8g). Furthermore, TEAD1 sequestered TAZ from Tip60, which resulted in increased acetylation and stability of Foxp3 (Fig. 8h and Supplementary Fig. 7d,e). In addition, knock-down of TEAD1 in naive CD4⁺ T cells resulted in decreased induction of T_{reg} cells, while overexpression of TEAD1 resulted in diminished T_H17 differentiation, but overexpression of a TAZ-unbound form of TEAD1 did not (Fig. 8i,j and Supplementary Fig. 7f). Give our results, we concluded that inactivation of Hippo signaling promoted translocation of TAZ nucleus, which was able to attenuate the function of Foxp3 and enhance RORγt-mediated T_H17 development. On the other hand, high expression of TEAD1 sequestered TAZ from RORγt and Foxp3 to positively promote T_{reg} cell differentiation (Supplementary Fig. 8).

DISCUSSION

In this study, we have revealed a physiological role for the transcriptional co-activator TAZ in the maintenance of T cell homeostasis. Notably, expression of a transgene encoding TAZ or activation of TAZ via depletion of TAZ-inhibitory components of Hippo signaling resulted in more T_H17 cells and fewer T_{reg} cells associated with autoimmune disease. Conversely, mice with TAZ-deficient T cells had more T_{reg} cells and were more resistant to the induction of T_H17 cell-dependent inflammatory disease. Therefore, TAZ represents a key regulator at the branch point of commitment to the T_{reg} cell lineage or T_H17 cell lineage that maintains immunotolerance. Both YAP and TAZ are homologous to Yorkie (Yki) in the *Drosophila* Hippo signaling pathway and act as co-activators of TEAD family of transcription factors of the Hippo pathway to control cell growth in mammals. However, we found that YAP expression in immune cells was very low, while TAZ expression was considerably induced during T cell differentiation. TAZ functioned as a co-activator of RORγt to promote T_H17 differentiation. However, TEAD1 inhibited T_H17 differentiation and positively regulated the development of T_{reg} cells by antagonizing the function of TAZ. Such data indicate distinct roles for TAZ and TEAD1 in commitment to the T_H17 cell lineage or T_{reg} cell lineage that are distinct from canonical Hippo signaling. Thus, it will be of particular interest to determine the expression, regulation and function of transcription factors of the TEAD family in the development of T_{reg} cells. Additionally, further work is needed to determine whether and which NDR kinases downstream of MST1 and MST2, including NDR1, NDR2, LATS1 and LATS2, are involved in the regulation of TAZ during T_H17 and T_{reg} cell differentiation.

Our current study has demonstrated that TAZ serves a vital role in T_H17 differentiation through several possible mechanisms. The first was that TAZ directly bound and activated RORγt and blocked the inhibitory effect of Foxp3 on RORγt to increase the expression of T_H17 signature genes and enhance T_H17 development. Second, TAZ attenuated the development of T_{reg} cells by diminishing Tip60-mediated acetylation of Foxp3 and targeting it for proteasomal degradation. In addition to interacting with TEAD1, TAZ has been linked to interactions with other transcription factors, including RUNX2 ('runt-related transcription factor 2')⁴⁶. Published studies have shown that RUNX1 can also promote T_H17 differentiation through enhancing the expression and activation of RORγt^{47,48}. It would be interesting to determine, in the future, the role of TAZ in Runx1-mediated T_H17 differentiation. Although TAZ functions mainly as a transcriptional co-activator, studies have also shown that it serves as a transcriptional repressor of gene transcription dependent on the transcription factor PPARγ (peroxisome proliferator-activated receptor-γ), including transcription of the gene encoding the inhibitory protein SOCS3 (ref. 9). SOCS3 negatively regulates IL-6 signaling^{49,50}, which is critical for T_H17 differentiation. Thus, it would be of interest to determine whether TAZ might promote IL-17 production via the repression of PPARγ-induced expression of SOCS3 or the activation of other transcription factors. MST1 deficiency in human and mice results in a complex combined immunodeficiency syndrome with autoimmune manifestations and recurrent bacterial and viral infections^{22,30}. That observation is reinforced by our finding that TAZ enhanced the differentiation of inflammatory T_H17 cells but attenuated the development of immunosuppressive T_{reg} cells, which supports the likely physiopathological relevance of the Hippo signaling pathway it engages. Thus, we propose that TAZ represents a previously unknown therapeutic target of particular relevance to tolerance and inflammation.

METHODS

Methods, including statements of data availability and any associated accession codes and references, are available in the [online version of the paper](#).

Note: Any Supplementary Information and Source Data files are available in the online version of the paper.

ACKNOWLEDGMENTS

We thank J. Avruch for comments on the manuscript. Supported by the National Basic Research Program (973) of China (2015CB910502 to L.C.), the National Natural Science Foundation of China (81422018 to L.C.; 31625010 and U1505224 to D.Z.; U1405225 and 81372617 to L.C.; J1310027 to D.Z.; 81472229 to L.H.; and 31600698 to J. Geng), the 111 Projects (B12001 and B06016), China's 1000 Young Talents Program (D.Z., and L.C.), the Fundamental Research Funds for the Central Universities of China-Xiamen University (20720160071 to D.Z. and 20720160054 to L.H.) and Major disease research projects of Xiamen (3502Z20149029 to L.C.). The funders had no role in study design, data collection and analysis, decision to publish, or preparation of the manuscript.

AUTHOR CONTRIBUTIONS

J. Geng, S.Y., H.Z., X.S., P.W., X.X., L.H., J. Gao, Y.S. and J.P. performed experimental biological research; X.L. provided human blood samples; C.X. performed mass-spectrometry analysis; R.L.J. provided mutant mice; D.Z. and L.C. conceived of the project, with input from R.L.J., N.X., L.L. and J.H., co-wrote the paper; and all authors edited the manuscript.

COMPETING FINANCIAL INTERESTS

The authors declare no competing financial interests.

Reprints and permissions information is available online at <http://www.nature.com/reprints/index.html>. Publisher's note: Springer Nature remains neutral with regard to jurisdictional claims in published maps and institutional affiliations.

1. Korn, T., Bettelli, E., Oukka, M. & Kuchroo, V.K. IL-17 and Th17 cells. *Annu. Rev. Immunol.* **27**, 485–517 (2009).
2. Littman, D.R. & Rudensky, A.Y. Th17 and regulatory T cells in mediating and restraining inflammation. *Cell* **140**, 845–858 (2010).
3. Bettelli, E. *et al.* Reciprocal developmental pathways for the generation of pathogenic effector TH17 and regulatory T cells. *Nature* **441**, 235–238 (2006).
4. Zhou, L. *et al.* TGF- β -induced Foxp3 inhibits T_H17 cell differentiation by antagonizing ROR γ function. *Nature* **453**, 236–240 (2008).
5. Xu, L., Kitani, A., Fuss, I. & Strober, W. Cutting edge: regulatory T cells induce CD4⁺CD25⁺Foxp3⁺ T cells or are self-induced to become Th17 cells in the absence of exogenous TGF- β . *J. Immunol.* **178**, 6725–6729 (2007).
6. Yang, X.O. *et al.* Molecular antagonism and plasticity of regulatory and inflammatory T cell programs. *Immunity* **29**, 44–56 (2008).
7. Zhou, X. *et al.* Instability of the transcription factor Foxp3 leads to the generation of pathogenic memory T cells *in vivo*. *Nat. Immunol.* **10**, 1000–1007 (2009).
8. Zhou, L., Chong, M.M. & Littman, D.R. Plasticity of CD4⁺ T cell lineage differentiation. *Immunity* **30**, 646–655 (2009).
9. Hong, J.H. *et al.* TAZ, a transcriptional modulator of mesenchymal stem cell differentiation. *Science* **309**, 1074–1078 (2005).
10. Kanai, F. *et al.* TAZ: a novel transcriptional co-activator regulated by interactions with 14-3-3 and PDZ domain proteins. *EMBO J.* **19**, 6778–6791 (2000).
11. Hong, W. & Guan, K.L. The YAP and TAZ transcription co-activators: key downstream effectors of the mammalian Hippo pathway. *Semin. Cell Dev. Biol.* **23**, 785–793 (2012).
12. Zanconato, F., Cordenonsi, M. & Piccolo, S. YAP/TAZ at the roots of cancer. *Cancer Cell* **29**, 783–803 (2016).
13. Varelas, X. *et al.* TAZ controls Smad nucleocytoplasmic shuttling and regulates human embryonic stem-cell self-renewal. *Nat. Cell Biol.* **10**, 837–848 (2008).
14. Varelas, X. *et al.* The Crumbs complex couples cell density sensing to Hippo-dependent control of the TGF- β -SMAD pathway. *Dev. Cell* **19**, 831–844 (2010).
15. Yu, F.X., Zhao, B. & Guan, K.L. Hippo Pathway in organ size control, tissue homeostasis, and cancer. *Cell* **163**, 811–828 (2015).
16. Pan, D. The hippo signaling pathway in development and cancer. *Dev. Cell* **19**, 491–505 (2010).
17. Harvey, K.F., Zhang, X. & Thomas, D.M. The Hippo pathway and human cancer. *Nat. Rev. Cancer* **13**, 246–257 (2013).
18. Johnson, R. & Halder, G. The two faces of Hippo: targeting the Hippo pathway for regenerative medicine and cancer treatment. *Nat. Rev. Drug Discov.* **13**, 63–79 (2014).
19. Halder, G., Dupont, S. & Piccolo, S. Transduction of mechanical and cytoskeletal cues by YAP and TAZ. *Nat. Rev. Mol. Cell Biol.* **13**, 591–600 (2012).
20. Avruch, J. *et al.* Protein kinases of the Hippo pathway: regulation and substrates. *Semin. Cell Dev. Biol.* **23**, 770–784 (2012).
21. Nehme, N.T. *et al.* MST1 mutations in autosomal recessive primary immunodeficiency characterized by defective naive T-cell survival. *Blood* **119**, 3458–3468 (2012).
22. Abdollahpour, H. *et al.* The phenotype of human STK4 deficiency. *Blood* **119**, 3450–3457 (2012).
23. Zhou, D. *et al.* The Nore1B/Mst1 complex restrains antigen receptor-induced proliferation of naive T cells. *Proc. Natl. Acad. Sci. USA* **105**, 20321–20326 (2008).
24. Katagiri, K., Imamura, M. & Kinashi, T. Spatiotemporal regulation of the kinase Mst1 by binding protein RAPL is critical for lymphocyte polarity and adhesion. *Nat. Immunol.* **7**, 919–928 (2006).
25. Katagiri, K., Maeda, A., Shimonaka, M. & Kinashi, T. RAPL, a Rap1-binding molecule that mediates Rap1-induced adhesion through spatial regulation of LFA-1. *Nat. Immunol.* **4**, 741–748 (2003).
26. Katagiri, K. *et al.* Crucial functions of the Rap1 effector molecule RAPL in lymphocyte and dendritic cell trafficking. *Nat. Immunol.* **5**, 1045–1051 (2004).
27. Katagiri, K. *et al.* Deficiency of Rap1-binding protein RAPL causes lymphoproliferative disorders through mislocalization of p27kip1. *Immunity* **34**, 24–38 (2011).
28. Li, J. *et al.* Mammalian sterile 20-like kinase 1 (Mst1) enhances the stability of Forkhead box P3 (Foxp3) and the function of regulatory T Cells by modulating Foxp3 acetylation. *J. Biol. Chem.* **290**, 30762–30770 (2015).
29. Dong, Y. *et al.* A cell-intrinsic role for Mst1 in regulating thymocyte egress. *J. Immunol.* **183**, 3865–3872 (2009).
30. Du, X. *et al.* Mst1/Mst2 regulate development and function of regulatory T cells through modulation of Foxo1/Foxo3 stability in autoimmune disease. *J. Immunol.* **192**, 1525–1535 (2014).
31. Katagiri, K. *et al.* Mst1 controls lymphocyte trafficking and interstitial motility within lymph nodes. *EMBO J.* **28**, 1319–1331 (2009).
32. Ueda, Y. *et al.* Mst1 regulates integrin-dependent thymocyte trafficking and antigen recognition in the thymus. *Nat. Commun.* **3**, 1098 (2012).
33. Nishikimi, A. *et al.* Rab13 acts downstream of the kinase Mst1 to deliver the integrin LFA-1 to the cell surface for lymphocyte trafficking. *Sci. Signal.* **7**, ra72 (2014).
34. Tang, F. *et al.* The kinases NDR1/2 act downstream of the Hippo homolog MST1 to mediate both egress of thymocytes from the thymus and lymphocyte motility. *Sci. Signal.* **8**, ra100 (2015).
35. Moroishi, T. *et al.* The Hippo pathway kinases LATS1/2 suppress cancer immunity. *Cell* **167**, 1525–1539 (2016).
36. Liu, B. *et al.* Toll receptor-mediated Hippo signaling controls innate immunity in *Drosophila*. *Cell* **164**, 406–419 (2016).
37. Geng, J. *et al.* Kinases Mst1 and Mst2 positively regulate phagocytic induction of reactive oxygen species and bactericidal activity. *Nat. Immunol.* **16**, 1142–1152 (2015).
38. Mou, F. *et al.* The Mst1 and Mst2 kinases control activation of rho family GTPases and thymic egress of mature thymocytes. *J. Exp. Med.* **209**, 741–759 (2012).
39. Jiao, S. *et al.* The kinase MST4 limits inflammatory responses through direct phosphorylation of the adaptor TRAF6. *Nat. Immunol.* **16**, 246–257 (2015).
40. Raab, M. *et al.* T cell receptor “inside-out” pathway via signaling module SKAP1-RAPL regulates T cell motility and interactions in lymph nodes. *Immunity* **32**, 541–556 (2010).
41. Li, W. *et al.* STK4 regulates TLR pathways and protects against chronic inflammation-related hepatocellular carcinoma. *J. Clin. Invest.* **125**, 4239–4254 (2015).
42. Guo, X. *et al.* Single tumor-initiating cells evade immune clearance by recruiting type II macrophages. *Genes Dev.* **31**, 247–259 (2017).
43. van Loosdregt, J. & Coffey, P.J. Post-translational modification networks regulating FOXP3 function. *Trends Immunol.* **35**, 368–378 (2014).
44. Lei, Q.Y. *et al.* TAZ promotes cell proliferation and epithelial-mesenchymal transition and is inhibited by the hippo pathway. *Mol. Cell. Biol.* **28**, 2426–2436 (2008).
45. Zhang, H. *et al.* TEAD transcription factors mediate the function of TAZ in cell growth and epithelial-mesenchymal transition. *J. Biol. Chem.* **284**, 13355–13362 (2009).
46. Azzolin, L. *et al.* YAP/TAZ incorporation in the β -catenin destruction complex orchestrates the Wnt response. *Cell* **158**, 157–170 (2014).
47. Zhang, F., Meng, G. & Strober, W. Interactions among the transcription factors Runx1, ROR γ t and Foxp3 regulate the differentiation of interleukin 17-producing T cells. *Nat. Immunol.* **9**, 1297–1306 (2008).
48. Lazarevic, V. *et al.* T-bet represses T(H)17 differentiation by preventing Runx1-mediated activation of the gene encoding ROR γ t. *Nat. Immunol.* **12**, 96–104 (2011).
49. Lang, R. *et al.* SOCS3 regulates the plasticity of gp130 signaling. *Nat. Immunol.* **4**, 546–550 (2003).
50. Croker, B.A. *et al.* SOCS3 negatively regulates IL-6 signaling *in vivo*. *Nat. Immunol.* **4**, 540–545 (2003).

ONLINE METHODS

Animals. The conditional knockout of *Mst1*, *Mst2*, *Taz* and *Yap1* has been previously described. *Taz*-transgenic mice were generated by Biocytogen (China). In brief, the pBS31-*Taz* plasmid was co-electroporated with a Flpe recombinase expression vector into ES cells that were expressing the M2rtTA tetracycline-responsive transactivator under control of the ROSA26 promoter. Transgene expression was induced by feeding the mice 2 mg/ml doxycycline in their drinking water supplemented with 10 mg/ml sucrose. For T cell-specific overexpression of TAZ, mice were crossed with mice expressing Cre under the control of the *Lck* promoter (*Lck-Cre*). Wild-type C57BL/6 mice, B6(Cg)-*Rorc*^{tm3Litt/J} mice (008771), *Stat3*^{tm1Xyfu} mice (016923), *Vav-Cre* mice (008610), *Lck-Cre* mice (003802) and *Ox40-Cre* mice (012839) were originally from the Jackson Laboratory. *Rag1*^{-/-} mice (B6.129S7-*Rag1tm1/Nju*) were purchased from Nanjing Biomedical Research Institute of Nanjing University. All mice were maintained under specific-pathogen-free conditions at the Xiamen University Laboratory Animal Center. All mouse experiments were approved by the Institutional Animal Care and Use Committee and were in strict accordance with good animal practice as defined by the Xiamen University Laboratory Animal Center.

Chemicals and reagents. Trichostatin A (T1952), nicotinamide (72345), ionomycin (10634), keyhole limpet hemocyanin (KLH, H7017), the phorbol ester PMA (P8139), DNase I (DN25) and MG132 (C2211) were from Sigma-Aldrich. Golgi-Stop was from BD. Oligo nucleotides were synthesized by Sangon Biotech (Supplementary Table 2).

Patients and specimens. Human blood specimens were obtained with from 22 subjects with rheumatoid arthritis, 21 subjects with Sjögren's syndrome and 18 healthy subjects at the First Affiliated Hospital of Xiamen University. Informed consent was provided by each subject before sample collection in accordance with the Declaration of Helsinki, and all procedures were approved by the ethics committee of Xiamen Health Science Center. Human memory CD4⁺ T cells were isolated with EasySep Human Memory CD4⁺ T Cell Enrichment Kit (StemCell Technologies).

KLH immunization. *Mst1*^{fl/fl}*Mst2*^{fl/fl}*Ox40-Cre* mice and *Taz*^{fl/fl}*Lck-Cre* mice and their littermates (6–8 weeks old; three per group) were immunized at the base of the tail (100 μl for each mouse) with KLH (0.5 mg/ml) emulsified in complete Freund's adjuvant (0.5 mg/ml). 7 d later, cells of spleen or the draining lymph nodes from KLH-immunized mice were stimulated with PMA and ionomycin in the presence of GolgiStop for 4 h, followed by intracellular cytokine staining (antibodies identified below ('Flow cytometry assays')). Stained cells were analyzed with a BD LSRFortessa flow cytometer (BD Biosciences) or a CyTOF mass cytometer (Fluidigm).

T cell-transfer colitis model. Splenocytes were collected from 6- to 10-week-old *Taz*^{fl/fl}*Lck-Cre*, *Taz* Tg, *Mst1*^{-/-}*Taz*^{fl/fl}*Lck-Cre* or control mice, and naive CD4⁺ T-cells were isolated using a Naive CD4⁺ T Cell Isolation Kit. A total of 4×10^5 CD4⁺CD44⁺CD62L⁺CD25⁻ cells were then adoptively transferred intraperitoneally into *Rag1*^{-/-} mice that were subsequently weighed every 7 d to evaluate IBD development. Mice were killed at 8–10 weeks after transfer when substantial weight loss occurred in the control groups. Colonic specimens from distal colons were analyzed by histopathology. Tissues were harvested and fixed overnight in 10% neutral-buffered formalin and were embedded in paraffin for sectioning. Hematoxylin and eosin staining was performed on 5-μm paraffin sections according to common methods. Lymphocytes were isolated from spleen, mesenteric lymph nodes and colonic LP and analyzed by flow cytometry.

EAE mouse model. EAE disease was induced with a MOG peptide of amino acids 35–55 in complete Freund's adjuvant. Mice were assigned scores daily on a scale of 0–5 in a double-blinded manner with the following criteria: 0, no disease; 1, tail paralysis; 2, wobbly gait; 3, hind limb paralysis; 4, forelimb paralysis; 5, moribund or dead. Gradations of 0.5 were assigned to mice exhibiting signs that fell between two of the scores listed above.

Isolation of ILP lymphocytes. Intestinal LP lymphocytes (LPLs) were prepared as described below. The small intestine and colon were dissected, fat

and Peyer's patches were removed, and tissues were washed in PBS and cut into pieces. The intestinal pieces were then treated for 30 min at 37 °C with medium containing 100 g/ml dithiothreitol (Sigma), 25 mM Hepes, 10% FBS (FBS) and 5 mM EDTA in RPMI1640 medium to remove epithelial cells, and were washed extensively with RPMI1640. Tissues were further digested in RPMI1640 containing 2% FBS, collagenase D (400 U/ml, Roche) and DNase I (0.1 mg/ml, Sigma) in a shaking incubator at 37 °C for 30 min. Cells were then layered on a 40–75% Percoll gradient (GE Healthcare), and lymphocyte-enriched populations were isolated from the cells at the 40%–75% interface after centrifugation at 2,000 r.p.m. for 20 min at room temperature. Lamina propria lymphocytes were washed twice, re-suspended in RPMI and used for further analysis.

Mass cytometry (CyTOF) assays. Single cells were washed and resuspended in Cell Staining Media (CSM; PBS with 0.5% BSA and 0.02% NaN₃). The cells were incubated with cisplatin (479306; Sigma-Aldrich) at 5 μM at room temperature for 10 min and were washed three times with CSM. For surface-maker staining, cells were blocked with antibody to CD16/CD32 (101302; BioLegend) and were incubated for 30 min at room temperature with a metal-labeled antibody cocktail according to the manufacturer's instructions, as follows: CD69-Nd143 (3143004B), CD4-Nd145 (3145002B), CD8-Nd146 (3146003B), CD25-Eu151 (3151007B), CD3e-Sm152 (3152004B), CD62L-Dy164 (3164003B), CD44-Yb171 (3171003B) and B220-176Yb (3176002B) (all from Fluidigm); CXCR5-148Nd (145502), CD138-154Sm (142502), GL7-156Gd (144602), PD-1-159Tb (109113), IgD-Tm169 (405737) and CD150-170Er (115933) (all from Biologend); and CD95-153Eu (14-0951-85 (from BD Bioscience); labeled with the indicated metal according to the manufacturer's instructions (Fluidigm). For intracellular staining, the cells were fixed and permeabilized with Maxpar Nuclear Antigen Staining Buffer Set (201063, Fluidigm) at room temperature for 30 min, were washed and resuspended in Nuclear Antigen Staining Perm (1×) buffer, and then were stained for 30 min at room temperature according to the manufacturer's instructions, as follows: IL-2-Nd144 (4144002B), Foxp3-Gd158 (3158003A), T-bet-Gd160 (3160010B), TNFa-DY162 (3162002B), IFN-γ-Ho165 (3165003B), IL-4-Er166 (3166003B), IL-17A-174Yb (3174002B) (all from Fluidigm); and BCL-6-150Nd (648302) (from Biologend); labeled with Nd according to the manufacturer's instructions (Fluidigm). After antibody staining, the cells were washed twice with CSM and then incubated for 10 min at room temperature (or overnight at 4 °C) with MAXPARNucleic Acid Intercalator-103Rh (DVS Sciences) in PBS with 1.6% formaldehyde. The cells were washed three times with CSM and once with PBS, diluted with water to $\sim 1 \times 10^6$ cells per ml, and filtered through a 40-μm membrane just before analysis by mass cytometry. Stained cells were then analyzed on a CyTOF mass cytometer (DVS Sciences) at an event rate of ~ 500 cells per second. The settings of the instrument and the initial post-processing parameters were described previously⁵¹. All mass cytometry FCS files were uploaded and evaluated using Cytobank software and established methods⁵². For viSNE analysis, total cells were analyzed and equal cell numbers were sampled from each FCS file.

Flow cytometry assays. Single cells isolated from the spleen, lymph nodes or intestinal LP were stained for 20 min with the appropriate fluorescence-conjugated antibodies (identified below) and washed, then were resuspended with flow cytometry staining buffer (1% BSA in PBS) containing 4',6-diamidino-2-phenylindole (DAPI; Invitrogen). For intracellular cytokine analysis, cells were re-stimulated with PMA (50 ng/ml) and ionomycin (1000 ng/ml) in the presence of Golgi-Stop (BD) for 4 h. Cells were then fixed and permeabilized with Intracellular Fixation & Permeabilization Buffer Set (eBioscience), and stained with anti-IFN-γ, anti-IL-4, anti-IL-17A (identified below). For the expression of Foxp3, cells were treated with the Foxp3 Staining Buffer Set (eBioscience) and stained with anti-Foxp3 (identified below). Stained cells were analyzed with a BD LSRFortessa flow cytometer (BD Biosciences). Flow cytometry data were plotted and quantified with FlowJo software (TreeStar). The following antibodies were used: APC-conjugated anti-CD3e (145-2C11, 0.2 mg/ml, 1:50), PerCP-Cy5.5-conjugated anti-CD4 (RM4-5, 0.2 mg/ml, 1:100), PE-Cy7-conjugated anti-CD4 (RM4-5, 0.2 mg/ml, 1:100), PerCP-Cy5.5-conjugated anti-CD8 (53-6.7, 0.2 mg/ml, 1:100), FITC-conjugated anti-CD44 (IM7, 0.5 mg/ml, 1:100), PE- or APC-conjugated anti-IFN-γ (XMG1.2, 0.2 mg/ml, 1:100), PE-Cy7- or anti-IL17A (TC11-18H10.1, 0.2 mg/ml, 1:100),

PE-conjugated anti-IL-17F (9D3.1C8, 0.2 mg/ml 1:100), Alexa 488-conjugated anti-Foxp3 (FJK-16S, 0.5 mg/ml, 1:200) and PE-Cy7-conjugated anti-IL-4 (11B11, 0.2 mg/ml, 1:200), all from BioLegend; PE-conjugated anti-Foxp3 (FJK-16S, 0.2 mg/ml, 1:100), APC-conjugated anti-CD25 (PC61.5, 0.2 mg/ml, 1:100) and FITC-conjugated anti-B220 (RA3-6B2, 0.5 mg/mL, 1:100), all from eBioscience; and PE conjugated anti-CD62L (MEL14, 0.2 mg/ml, 1:100), from BD Bioscience.

Cell culture. The 293T and HeLa cell lines (from the American Type Culture Collection) were tested for mycoplasma contamination and were found to be negative for this. 293T and HeLa cell lines were cultured in DMEM supplemented with 10% FBS and 1× penicillin-streptomycin (Invitrogen). Lymphocytes were cultured in RPMI1640 complete medium with 10% FBS (Gibco), 1 mM sodium pyruvate (Gibco), 50 μM β-ME and 1× penicillin-streptomycin (Invitrogen).

CFSE labeling. CD4⁺ cells were labeled for 8 min at 37 °C with 2.5 μM carboxyfluorescein diacetate succinimidyl ester (CFSE) according to the manufacturer's instructions (Invitrogen), were washed three times with RPMI1640 and were activated with plate-bound anti-CD3 (2 μg/ml; 100314, BioLegend) and anti-CD28 (2 μg/ml; 122004, BioLegend) in complete medium for 48 h, followed by flow cytometry.

Mouse T cell differentiation. Naive CD4⁺ T cells were prepared from the spleen and lymph nodes of mice using the Naive CD4⁺ T Cell Isolation Kit (130-104-453, Miltenyi Biotec) (purity was 97%). Cells were activated by plate-bound anti-CD3 (2 μg/ml; 100314; BioLegend) and anti-CD28 (2 μg/ml; 122004; BioLegend) in the presence of TGF-β (2.5 ng/ml; 580706; BioLegend), IL-6 (30 ng/ml; AF-216-16; Peprotech), anti-IL-4 (10 μg/ml; 504115; BioLegend) and anti-IFN-γ (10 μg/ml; 505827; BioLegend). For T_H17 polarization; TGF-β (2.5 ng/ml; 580706; BioLegend), for T_{reg} cell polarization; IL-12 (10 ng/ml; 419-ML-050; R&D system) and anti-IL-4 (10 μg/ml; 504115; BioLegend), for T_H1 polarization; or IL-4 (50 ng/ml; 404-ML-010; R&D system), anti-IL-12 (10 μg/ml; 505305; BioLegend) and anti-IFN-γ (10 μg/ml; 505827; BioLegend), for T_H2 polarization.

Human T cell culture and differentiation. Mononuclear cells were prepared from the blood of healthy adult donors on Ficoll PAQUE gradients (GE). Human Naive CD4⁺ T cells were isolated with n EasySep Human Naive CD4⁺ T Cell Isolation Kit (Stemcell technologies). Cells were cultured in X-VIVO serum-free medium (Lonza) supplemented with gentamycin. CD4⁺ T cells were seeded at a density of 1 × 10⁶ cells per ml in U-bottomed 96-well plates with pre-coated with anti-CD3 (2 μg/ml; 300314, BioLegend) and anti-CD28 (2 μg/ml; 302914, BioLegend) and were incubated at 4 °C overnight. For long-term experiments, cells were split as needed on day 3. For T_H1 and T_H2 cell differentiation, ImmunoCult Human T_H1 Differentiation Supplement and ImmunoCult Human T_H2 Differentiation Supplement (Stemcell technologies) were added at day 0 and were maintained throughout the experiment. For T_{reg} cell differentiation, IL-2 (10 U/ml, 100-12-10; Shenandoah), TGF-β1 (2.5 ng/ml; 240-B-010; R&D Systems) and neutralizing antibodies to IL-4 (1 μg/ml; 500815; BioLegend) and IFN-γ (1 μg/ml; 506513; BioLegend) were added at day 0 and were maintained throughout the experiment. For T_H17 differentiation, IL-1β (10 ng/ml; 201-LB-025; R&D Systems), IL-6 (10 ng/ml; 206-IL-010; R&D Systems), IL-21 (10 ng/ml; 8879-IL-010; R&D Systems), IL-23 (10 ng/ml; 1290-IL-010; R&D Systems), TGF-β1 (2.5 ng/ml) and neutralizing antibodies to IL-4 (1 μg/ml) and IFN-γ (1 μg/ml) were added at day 0 and were maintained throughout the experiment. Cells were collected on day 6 for real-time PCR analysis and immunoblot analysis.

Regulatory T cell inhibition assays. CFSE labeled wild-type CD4⁺CD25⁻ responder T cells (1 × 10⁵) were cultured for 2–4 d in U-bottomed 96-well plates with control T cells (CD4⁺CD25⁻) or with T_{reg} cells (CD4⁺CD25⁺), at various ratios, in the presence of soluble anti-CD3 (1 μg/ml; 100314; BioLegend) and 4 × 10⁵ irradiated (4,000 rads) splenocytes from wild-type mice were added to the co-culture as antigen-presenting cells instead of anti-CD28. T_{reg} cells were isolated from spleen and lymph nodes of wild-type or TAZ-cKO mice using an EasySep Mouse CD4⁺CD25⁺ Regulatory T Cell Isolation Kit II (Stemcell

technologies). Proliferation was assayed by CFSE dilution, and IL-2 production in culture was measured with ELISA kit.

Cytokine measurement. Cell supernatants were collected at the appropriate time points during culture. The concentrations of mouse IL-17, and IFN-γ were measured with ELISA kits (BioLegend) according to the manufacturer's instructions.

Retroviral packaging and transduction. shRNA-containing oligonucleotides (TEAD1-specific and control shRNAs, **Supplementary Table 1**) were cloned into retroviral vector dLMP containing IRES-regulated GFP. Genes encoding wild-type TAZ, TAZ(S51A), TAZ(S89A) and TAZ(S89A,S51A) were cloned into retroviral vector pMIG containing IRES-regulated GFP, respectively. Plat-E packaging cells were transfected with 3 μg of retroviral vector along with 9 μl of TransIT-LT1 transfection reagent (Mirus). 48 h after transfection, the culture supernatant containing retrovirus was collected. Naive CD4⁺ T cells from wild-type or TAZ-cKO mice were activated with plate-bound anti-CD3 and anti-CD28 in the presence or absence of 2.5 ng/ml TGF-β or 30 ng/ml IL-6 or combination of these stimuli. 24 h after stimulation, CD4⁺ T cells were infected with retrovirus together with 8 μg/ml polybrene and 100 U/ml IL-2 by centrifugation of cells at 2,000 r.p.m. for 60 min at room temperature. 3 d after infection, the cells were re-stimulated with PMA and ionomycin in the presence of Golgi-Stop for 5 h, followed by intracellular cytokine staining (antibodies identified above) and flow cytometry analysis.

Lentivirus packaging and infection. Lentivirus was packaged by co-transfection in 293T cells with shRNA (Smad3-specific and control shRNAs, **Supplementary Table 2**) in the vector pL3.7, VSV-G and Δ8.9 plasmids by Lipofectamine 2000 (Invitrogen). Viral supernatants were harvested at 48h after transfection, then were passed through a 0.45-μm filter and diluted 2:3 with fresh medium containing 8 μg/ml polybrene and were used to infect the target cells at 80% confluence. Protein expression was visualized by immunoblot analysis.

Transfection and luciferase reporter assay. Cells cultured in 12-well plates were transfected with the plasmids indicated in the main body of the text using Lipofectamine 2000 (Invitrogen). At 48 h after transfection, cells were washed with PBS and lysed in Reporter Lysis Buffer (Invitrogen). Luciferase reporter activities were measured in triplicate using the Dual-Luciferase reporter assay system (Promega, Madison, WI, USA), according to the manufacturer's protocol, and quantified using the GloMax 96-well plate luminometer (Promega). The firefly luciferase to *Renilla* luciferase ratios were determined and were defined as the relative luciferase activity.

Chromatin immunoprecipitation. Chromatin immunoprecipitation (ChIP) assays were performed according to the protocol of the CHIP assay kit (Upstate Biotechnology Inc., NY, USA) as previous described⁵³. In brief, T_H17 cells were fixed with 1% formaldehyde for 10 min at room temperature (RT) and then were quenched with glycine (125 mM) for 5 min. The fixed cells were washed with PBS containing protease inhibitors and were lysed in lysis buffer (pH 8.1) containing 1% SDS, 10 mM EDTA, 50 mM Tris-HCl, and protease inhibitors, for 10 min on ice before the sonication, centrifugation and addition of dilution buffer. 1% of input was removed, and the lysates were immunoprecipitated with 10 μl of anti-Smad3 (5339S, CST), 10 μl of anti-Stat3 (9139, CST), or 2 μl of Normal Rabbit IgG (2729, CST) for 6 h. Salmon sperm DNA-protein A/G-Sepharose beads were added to the immunoprecipitation samples containing anti-Smad3, anti-STAT3 or IgG (control) for incubation overnight. Immunocomplexes were washed sequentially with low-salt buffer, high-salt buffer, LiCl buffer and twice with TE before elution in 200 μl of elution buffer (1% SDS, 0.1M NaHCO₃). The elutes were heated at 65 °C for 4 h to reverse the cross-linking and were treated with RNase A for 30 min at 37 °C, followed by treatment with proteinase K for 1 h at 45 °C, to remove RNA and protein. DNA was recovered using a QIAGEN PCR purification kit and was eluted in 50 μl of QIAGEN EB buffer (QIAGEN, Hilden, Germany). 1% of input and 10% of the immunoprecipitates were used in PCR analyses using AmpliTaq Gold DNA polymerase (Applied Biosystems, CA, USA) for 30 cycles at 95 °C for 30 s, 58 °C for 30 s, 72 °C for 60 s (after an initial denaturation for 10 min at 95 °C). The primers used for ChIP are in **Supplementary Table 1**.

Ubiquitination assay. 293T cells were transfected for 36 h with the appropriate plasmids and were lysed in ice-cold lysis buffer (‘‘TNTE 0.5%’’: 50 mM Tris-HCl, pH 7.5, 150 mM NaCl, 1 mM EDTA and 0.5% Triton X-100, containing 10 mM NaF, 2 mM Na₃VO₄, 10 mg/ml leupeptin and 1 mM PMSF). The cell lysates were subjected to immunoprecipitation with anti-Flag (identified below), were eluted by boiling 10 min in 1% SDS, were diluted ten times in lysis buffer TNTE 0.5% and then underwent re-immunoprecipitation with anti-Flag (2 × IP). The ubiquitin-conjugated proteins were detected by immunoblot analysis with the appropriate antibodies (identified below).

Immunoblot analysis. Cells were lysed in cell lysis buffer containing 150 mM NaCl, 0.1 mM EDTA, 5% glycerol, 10% Triton-100, 10 mM and a ‘cocktail’ of protease inhibitors. Proteins were separated by SDS-PAGE, transferred onto a PVDF membrane and then identified by immunoblot analysis with the appropriate primary antibodies at a dilution of 1:1,000 (or as stated otherwise below). anti-phosphorylated Stat3 (9145), anti-phosphorylated Smad3 (9520), anti-STAT3 (9139), anti-Smad3 (9523), anti-ubiquitin (3936), anti-ubiquitinK48 (8081), anti-GAPDH (5174), anti-TAZ (4883) and anti-DYKDDDDK (14793), all from Cell Signaling Technology; anti-HA (sc-7392, sc-805), anti-GFP (sc-8334), anti-Octa (sc-166355), anti-Foxp3 (sc-28705), anti-RORγt (sc-14196) and anti-Myc (sc-40), all from Santa Cruz; anti-K-Ace (#05-515), from Millipore; anti-KAT5 (10827-1-AP), from Proteintech; and horseradish peroxidase-conjugated antibody to rabbit IgG (7074) or to mouse IgG (7076) (1:3,000 dilution for each), from Jackson ImmunoResearch Laboratories. The protein bands were visualized with a SuperSignal West Pico Kit according to the manufacturer’s instructions (Thermo Fisher Scientific Pierce).

Confocal fluorescence microscopy. HeLa cells seeded on cover slips in six-well dish with 30% confluence were transfected with the appropriate constructs and were cultured for another 24 h. The cells were washed three times with PBS and were fixed for 15 min at room temperature with 4% (vol/vol) paraformaldehyde, after which additional immunofluorescence staining was applied. For staining with anti-DYKDDDDK (Flag) tag (1:250 dilution; 14793; CST) or anti-HA tag (1:250 dilution; sc-7392; Santa Cruz), then fixed cells were rinsed with PBS and then incubated for 10 min on ice with 0.2% Triton X-100 and 0.2% BSA in PBS. Following permeabilization, nonspecific binding in the cells was blocked by incubation for 30 min at room temperature with 0.02% Triton X-100 and 5% BSA in PBS and cells were incubated for 3 h with specific primary antibodies (identified above). After three washes with PBS, the cells were incubated for another 1 h with secondary antibodies (1:250, Alexa Fluor 555-conjugated anti-mouse IgG (A31570) or Alexa Fluor 647-conjugated anti-rabbit IgG (A21246); both from Invitrogen). Subsequently, the

cells were washed three times with PBS and were mounted with Vectashield mounting medium containing DAPI. All images were collected with a Precision DeltaVision-OMX Super-Resolution Microscope (GE OMX V4).

Mass spectrometry. After staining of gels with Coomassie blue, excised gel segments were subjected to in-gel trypsin digestion and dried. Peptides were dissolved in 10 μl 0.1% formic acid and were auto-sampled directly onto a 100-μm × 10-cm fused silica emitter made in-house and packed with reversed-phase Reprosil-PurC18-AQ resin (3 μm and 120 Å; Ammerbuch). Samples were then eluted for 60 min with linear gradients of 5–32% acetonitrile in 0.1% formic acid at a flow rate of 300 nl/min. Mass spectra data were acquired with a TripleTOF 5600+ mass spectrometer (AB Sciex) equipped with a nano-electrospray ion source. Data were collected at an IDA mode. The wiff files were searched with the ProteinPilot (Version 4.5) against a database from the Uniprot protein sequence database.

Quantitative real-time PCR. Following isolation with TRIzol reagent (Invitrogen), mRNA was specifically purified with a RNAeasy Mini Kit (Qiagen). First-strand cDNA was then obtained with the PrimeScript RT reagent Kit with gDNA Eraser (Takara). Real-time quantitative PCR was performed using SYBR Premix Ex TaqII (Takara) and the Bio-Rad iCycler iQ system (Bio-Rad, Hercules, CA, USA). All runs were accompanied by the internal control gene *Gapdh*. The samples were run in triplicate and normalized to GAPDH using a ΔΔ cycle threshold-based algorithm, to provide arbitrary units representing relative expression levels. The primer sequences for specific genes are in **Supplementary Table 2**.

Statistical analysis. All statistical analyses were performed with Prism5 software (GraphPad Software). Student’s *t*-test was used for comparisons between two groups. The relative expression levels of RORC and TAZ in memory CD4⁺ T cells isolated from blood of patients were plotted, and the linear regression *t*-test was applied. A *P* value of less than 0.05 was considered statistically significant.

Data availability. The data that support the findings of this study are available from the corresponding author upon request.

- Bendall, S.C. *et al.* Single-cell mass cytometry of differential immune and drug responses across a human hematopoietic continuum. *Science* **332**, 687–696 (2011).
- Amir, A.D. *et al.* viSNE enables visualization of high dimensional single-cell data and reveals phenotypic heterogeneity of leukemia. *Nat. Biotechnol.* **31**, 545–552 (2013).
- Wu, H. *et al.* The Ets transcription factor GABP is a component of the hippo pathway essential for growth and antioxidant defense. *Cell Rep.* **3**, 1663–1677 (2013).